February 2017 extreme Saharan dust outbreak in the Iberian Peninsula: from lidar-derived optical properties to evaluation of forecast models

Alfonso J. Fernández[1], Michäel Sicard[2,3], Maria J. Costa[4], Juan L. Guerrero-Rascado[5,6], José L. Gómez-Amo[7], Francisco Molero[1], Rubén Barragán[2,3], Daniele Bortoli[4], Andrés E. Bedoya-Velásquez[5,6], María P. Utrillas[7], Pedro Salvador[1], María J. Granados-Muñoz[2], Miguel Potes[4], Pablo Ortiz-Amezcua[5,6], José A. Martínez-Lozano[7], Begoña Artíñano[1], Constantino Muñoz-Porcar[2], Rui Salgado[4], Roberto Román[5,6], Francesc Rocadenbosch[2,3], Vanda Salgueiro[4], José A. Benavent-Oltra[5,6], Alejandro Rodríguez-Gómez[2], Lucas Alados-Arboledas[5,6], Adolfo Comerón[2] and Manuel Pujadas[1].

[1]Dept. of Environment, Research Centre for Energy, Environment and Technology (CIEMAT), Madrid, Spain.

[2]Dept. of Signal Theory and Communications, CommSensLab, Universitat Politècnica de Catalunya, Barcelona, Spain.

[3]Ciències i Tecnologies de l'Espai - Centre de Recerca de l'Aeronàutica i de l'Espai / Institut d'Estudis Espacials de Catalunya (CTE-CRAE / IEEC), Universitat Politècnica de Catalunya, Barcelona, Spain

[4]Institute of Earth Sciences and Dept. of Physics, ECT and IIFA, Universidade de Évora, Évora, Portugal.

[5]Dept. of Applied Physics, University of Granada, Granada, Spain.

[6]Andalusian Institute for Earth System Research (IISTA-CEAMA), Granada, Spain.

[7]Dept. of Physics of the Earth and Thermodynamics, University of Valencia, Valencia, Spain.

Correspondence to: Alfonso Javier Fernández (alfonsoj.fernandez@ciemat.es)

Abstract

An unprecedented extreme Saharan dust event was registered in winter time from 20 to 23 February 2017 over the Iberian Peninsula (IP). We report on aerosol optical properties observed under this extreme dust outbreak through remote sensing (active and passive) techniques. For that, EARLINET (European Aerosol Research LIdar NETwork) lidar and AERONET (AErosol RObotic NETwork) Sun-photometer Cimel CE 318 measurements are used. The sites considered are: Barcelona (41.38ºN, 2.17ºE), Burjassot (39.51ºN, 0.42ºW), Cabo da Roca (38.78ºN, 9.50ºW), Évora (38.57ºN, 7.91ºW), Granada (37.16ºN, 3.61ºW) and Madrid (40.45ºN, 3.72ºW).

In general, large aerosol optical depths (AOD) and low Ångström exponents (AE) are observed. An AOD of 2.0 at 675 nm is reached in several stations. Maximum values of AOD$_{675}$ of 2.5 are registered in Évora. During and around the peak of AOD$_{675}$, AEs close to 0 are measured. With regard to vertically-resolved aerosol optical properties, particle backscatter coefficients as high as $1.5\cdot10^{-5}$ m^{-1} sr^{-1} at 355 nm are recorded at every lidar stations. Mean lidar ratios are found in the range 40 - 55 sr at 355 nm and 34 - 61 sr at 532 nm during the event inside the dust layer. Mean particle and volume depolarization ratios are found to be very consistent between lidar stations. They range 0.19-0.31 and 0.12-0.26 respectively. The optical properties are also found very stable with height in the dust layer. Another remarkable aspect of the event is the limited height of the dust transport which is found between the ground and 5 km. Our vertically-resolved aerosol properties are also used to estimate the performances of two dust models, namely BSC-DREAM8b and NMMB/BSC-Dust, in order to evaluate their forecast skills in such intense dust outbreaks. We found that forecasts provided by the NMMB/BSC-Dust show a better agreement with observations than the ones from BSC-DREAM8b. The BSC-DREAM8b forecasts (24 h) present a large underestimation during the event. No clear degradation of the prognostics is appreciated in 24, 48, 72 h except for the Barcelona station.

1 Introduction

Mineral aerosols are usually originated over arid or semiarid regions as a consequence of continuous soil erosion produced by wind. The strong warming of desert areas during daytime produces vertical thermal turbulences that can reach altitudes of up to 5000 m, followed by periods of nocturnal stability (Santos et al. 2013). Massive resuspension of huge amounts of mineral aerosols are thus produced and can be transported long distances by different mechanisms. 40% of aerosol mass emitted into the troposphere is attributed to desert dust and it is considered as the second largest source of natural aerosols (Andreae 1995, Salvador et al. 2014). One of the main desert dust sources is the Sahara desert since it is responsible for more than half of the world atmospheric mineral dust (Prospero et al. 2002, Mahowald et al. 2005, Wagner et al. 2009, Salvador et al. 2016). Under specific synoptic meteorological situations, a large amount of Saharan dust is transported towards the Mediterranean basin (Lafontaine et al. 1990, Obregón et al. 2015, Cuevas et al. 2017).

Lately, the number of surveys which address the study of atmospheric mineral aerosols has been increased for several reasons. Firstly, from the climate change standpoint, mineral aerosols play an important role on atmospheric radiative budget through scattering and absorption of the incoming solar and outgoing infrared radiation, and acting as cloud condensation nuclei (Ansmann et al. 2005, Klein et al. 2010, IPCC 2013). Currently, the large temporal and spatial variability is responsible for a high uncertainty degree in aerosol radiative forcing estimates (Boucher et al. 2013) (Forster et al. 2007). Furthermore, there is a lack of systematic statistical surveys during a long time period. Some of them, (Mona et al. 2006) (Salvador et al. 2013) (Pey et al. 2013), have indicated that the Mediterranean basin is affected by African dust outbreaks following a marked seasonal pattern. Summer prevalence has been detected in the western side (Sicard et al. 2016), no seasonal trend has been observed in the central region and higher contributions of desert dust have been commonly produced in spring-early summer in the eastern side of this basin.

Winter is the season when these phenomena are less likely to occur across the whole Mediterranean basin (Querol et al. 2009). However, extreme dust outbreaks, as the one described in this paper or others that took place quite recently (Cazorla et al. 2017, Sorribas et al. 2017), occurred during the coldest season. According to the fifth IPCC (2013) report an extreme weather event can be defined as a rare phenomenon taking into account its historical statistical distribution for a particular place and/or time. Then 10th and 90th percentiles are usually considered as reference to define "rare". In the supplementary material: Fig. S1, S2, S3 and Table S1, percentile of AOD_{675} and Ångström exponent (440-870 nm) are presented having considered all data available at each station in the Iberian Peninsula. Along with it, data concerning this event is also represented in order to justify its extreme character. This is important to be highlighted as extreme weather events have been discussed and suggested to be connected to climate change. For instance some remaining questions concern whether or not such events take place earlier or later in the season or if their severity has been increased (World Meteorological Organization 2011).

What is more, it has been demonstrated that African dust is the main source contributing to the regional background levels of PM_{10} (particular matter with an aerodynamic diameter lower than 10 µm) across the Mediterranean (35-50% of PM_{10}) with maximum contributions up to 80% of the total PM_{10} mass (Pey et al. 2013) . These sporadic but intense natural contributions of PM have been responsible of a high number of exceedances of the PM_{10} daily limit value (50 $\mu g/m^3$, after the 2008/50/EC European Directive) as registered in different rural and urban monitoring sites across the

Mediterranean Basin (Querol et al. 2009, Salvador et al. 2013). Moreover, statistically significant evidences on the association between short-term exposure to desert dust and health outcomes have also been derived (Karanasiou et al., 2012). PM_{10} originating from the desert was positively associated with mortality and hospitalizations in 13 Southern European cities for the period 2001-2010 (Stafoggia et al. 2016). A recent regional study carried out in Spain has associated PM_{10} levels with daily mortality during African dust outbreaks in most of the Spanish regions (Díaz et al. 2017).

In addition, massive aerosol emissions into the atmosphere can be an issue for aircraft operation. For instance, aircraft engines, that fly through atmospheres with significant mineral dust loads on a regular basis, usually undergo an accelerated aging, and as a result, an anticipated and unexpected overhaul and maintenance is required (Weinzierl et al. 2012). In addition, atmospheric mineral dust can cause a huge impact on aviation by reducing the visibility during the landing and takeoff of aircrafts (Weinzierl et al. 2017).

For all these reasons, characterizing these events in detail is strictly necessary given the aforementioned implications on human society. In this article, we report on a record-breaking dust event that hit the Iberian Peninsula (IP) on 20 - 23 February 2017. The observational task has been carried out through remote sensing techniques at different sites located in the IP. Sun and sky scanning spectral radiometers and lidar measurements have provided observations concerning the spatial (vertical and horizontal) distribution of aerosol. In this sense, the lidar technique is indispensable since it can provide both temporally and vertically resolved dust layering structures. To give an idea of the magnitude of the extreme event it is noteworthy to state that the AOD was greater than 2 at 675 nm in several AERONET stations and for the most intense periods some lidar and sun-photometer retrievals could not be performed due to high aerosol load, respectively, attenuating the lidar signal and blocking the sun. A previous work concerning such event at the IP found an AODs at 500 nm up to 1.5 in the south of Spain (Guerrero-Rascado et al. 2009). In this case, maximum values of particle backscatter coefficients ($1.5 \cdot 10^{-5}$ m^{-1} sr^{-1} at 355 nm) were similar to those registered during this event, however it took place in September. Preissler et al. (2011) reported an aerosol optical thickness up to 2 in Portugal as a consequence of another extreme dust outbreak episode in April (Preissler et al. 2011).

Finally, having the capability to forecast such events is also very important. Comparison exercises between real and modeled data must be done in order to better comprehend extreme dust events but more importantly to provide accurate information to decision makers beforehand. Because of that, it has been checked if the results from dust models (BSC-DREAM8b and NMMB/BSC-Dust) are in agreement with observations as the relationship between certain meteorological patterns and extreme African dust events can provide useful information for human health, air traffic controllers, or to predict different climate change scenarios. However, dust models have proved to fail in certain occasions under extreme dust events (Mamouri et al. 2016) mainly because the scale used by models is not small enough to appreciate such phenomena.

The aim of this paper is to procure an overview of the available dust observations obtained from remote sensing techniques at different locations in the IP, to derive the aerosol optical property profiles from such observations and to compare them against the results computed from models. The paper is organized as follows. The instruments and methodology are briefly described in Sect. 2. Sect. 3 deals with the description of the synoptic situation and columnar aerosol optical properties from sun and sky spectral radiometers. In section 4, vertically-resolved optical properties are discussed. Section 5 presents the performance of the dust models. Finally, conclusions can be found in Sect. 6.

2 Instruments and methodology

2.1 AERONET CIMEL CE-318 Sun-photometers in the IP.

The AErosol RObotic NETwork (AERONET) is a global ground-based network of sun/sky multi-wavelength CIMEL CE-318 sun-photometers that provides relatively long-term records of atmospheric columnar aerosol optical properties (Holben et al. 1998). The CIMEL spectral sun-photometer measures the direct solar irradiances with a field of view of approximately 1.2° and the sky radiances (in the almucantar and principal plane scenarios), at several spectral channels (see table 1). The direct-sun measurements are used to obtain the spectral AOD, Ångström exponent at several wavelength pairs and precipitable water vapor, approximately every 15 min. The estimated AOD uncertainty (mainly due to the calibration) is between 0.01 and 0.02 (Holben et al. 1998).

The sky radiance measurements can be inverted to estimate aerosol optical properties such as the size distribution, the percentage of spherical particles in the aerosol mixture, several microphysical parameters describing the total, fine and coarse aerosol modes and numerous spectral quantities: complex refractive index, single scattering albedo, phase function, asymmetry parameter, extinction and absorption optical depths. The aerosol properties retrieved are hence used for calculating the broad-band fluxes at the bottom and top of the atmosphere, the radiative forcing and forcing efficiencies are also provided. A detailed description of the version 2 AERONET inversion products is given by (Holben et al. 2001). Table 1 shows the six AERONET stations distributed in the IP that were considered in this study. In figure 2 these places are located on a map.

Table 1 – Summary of the sites considered in the study, main characteristics of the AERONET sun-photometers and EARLINET lidars used, and lidar measurement time.

Site	Long. (º)	Lat. (º)	Altitude (m a.s.l.)	AERONET Sun photometer channels for AOD (nm)	EARLINET Lidar channels (nm)			Lidar measurement time	
					Elastic	Raman	Vertical resol. (m)	Start time	Stop time
Barcelona	2.11° E	41.39° N	115	440, 675, 870, 1020	355, 532 total, 532 cross, 1064	387, 407, 607	3.75	08:11 UTC (23 Feb)	23:54 UTC (23 Feb)
Burjassot	0.42° W	39.51° N	60	340, 380, 440, 500, 675, 870, 1020, 1640	355 cross and parallel	387	15	-	-
Cabo da Roca	9.50° W	38.78° N	140	340, 380, 440, 500, 675, 870, 1020	-			-	-
Évora	7.91° W	38.57° N	293	340, 380, 440, 500, 675, 870, 1020	355, 532, 532 cross, 1064	387, 607	30	00:00 UTC (20 Feb)	23:59 UTC (23 Feb)
Granada	3.61° W	37.16° N	680	340, 380, 440, 500, 675, 870, 1020	355, 532 parallel, 532 cross, 1064	387, 407, 607	7.5	12:00h UTC (20 Feb)	18:00h UTC (20 Feb)
								19:00h UTC (20 Feb)	21:00h UTC (20 Feb)
								07:31h UTC (21 Feb)	14:21h UTC (21 Feb)
								07:31h UTC (22 Feb)	20:00h UTC (22 Feb)
Madrid	3.72° W	40.45° N	669	340, 380, 440, 500, 675, 870, 1020	355, 532, 1064	387, 407, 607	7.5 (elastic), 3.75 (Raman)	21:00h UTC (22 Feb)	23:36h UTC (22 Feb)
								05:00h UTC (23 Feb)	08:00h UTC (23 Feb)
								11:00h UTC (23 Feb)	11:52h UTC (23 Feb)

2.2 EARLINET lidars in the IP

The European Aerosol Research Lidar Network, EARLINET, aims at creating a quantitative, comprehensive, and statistically significant database for the horizontal, vertical, and temporal distribution of aerosols on a continental scale, providing the most extensive collection of ground-based data for the aerosol vertical distribution over Europe (Pappalardo et al. 2014). In this work four Iberian EARLINET stations (Barcelona, Madrid, Évora and Granada) provided lidar data, all of them equipped with multi-wavelength lidars and some of them with depolarization capabilities (see Table 1). Burjassot lidar station was not available at this moment.

On a regular basis, the EARLINET protocol establishes that lidar measurements have to be carried out on Monday (at 14 UTC and at sunset) and on Thursday (sunset). However, under exceptional events, as the one described in this work, these stations perform additional measurements in order to register the phenomena as long as possible. Then, lidar signals were averaged over 30 or 60 minute periods in order to guarantee a proper signal-to-noise ratio throughout the vertical column. The criteria followed to choose such periods is based on the representation of the dust plume but also on the data availability at atmospheric levels where Rayleigh computation can be accomplished since the aerosol burden during this event was certainly high and produced a great radiation extinction, which hampered the Rayleigh retrieval. In this work, lidar measurements at each station were performed at the periods specified in Table 1.

Vertically resolved particle coefficients were derived by means of the Klett-Fernald algorithm (Klett 1981, Fernald 1984). This algorithm requires an assumption of the lidar ratio (LR), defined as the particle extinction (α) to particle backscatter (β) coefficients ratio, and for mineral dust we have considered a value of 50 sr (Guerrero-Rascado et al. 2008, Guerrero-Rascado et al. 2009, Muller et al. 2009, Muller et al. 2010, Preissler et al. 2011). If possible, α and β coefficient profiles were retrieved independently (Ansmann et al. 1992), which in turn allow computing the vertically-resolved LR. Given the fact that the LR is an intensive parameter, it provides useful information for the analysis of aerosol optical properties. Another intensive variable is the Ångström exponent (Ångström 1964). It is inversely related to the size of particles: the greater the exponent is, the smaller the particles are and vice versa (Amiridis et al. 2009). This is defined for the wavelength pair (λ_1 and λ_2) as:

$$\mathring{a}_{\alpha} = -\frac{\log\left[\frac{\alpha(\lambda_1)}{\alpha(\lambda_2)}\right]}{\log\left[\frac{\lambda_1}{\lambda_2}\right]} \qquad (1)$$

Since extinction coefficients were not always available, Ångström exponent was only obtained for such cases. However, the three backscatter coefficients were always estimated, which allowed to retrieve, the backscatter-related Ångström exponent. For this reason this parameter is also estimated, and the relationship to the aerosol size is similar than the previous definition, although it is affected by other parameters such as refractive index so the relationship should not be straightforward. Last but not least, lidar systems equipped with depolarization channels procure relevant information about the aerosol type because backscatter signals related to the cross and parallel-polarized component varies depending on aerosol shape.

With regard to the errors associated to the measurements, we made use of the Monte-Carlo technique so as to estimate the uncertainties of the vertically-resolved backscatter and extinction coefficients. This technique is based on the random extraction of new lidar signals, each bin of which is considered a sample element of a given probability distribution with the experimentally observed mean value and standard deviation. The extracted lidar signals are then processed with the same algorithm to obtain a set of solutions from which the standard deviation is inferred as a function of height (Pappalardo et al. 2004).

2.3 Description of the models evaluated and methodology

The present analysis utilizes the operational 72-hour dust forecasts of the BSC-DREAM8b (Perez et al. 2006, Basart et al. 2012) and the NMMB/BSC-Dust (Perez et al. 2011) models (http://www.bsc.es/ess/information/bsc-dust-daily-forecast) for the period from 19 to 22 February 2017. Both models are developed and operated at the Barcelona Supercomputing Center (BSC). Table 2 summarizes the main parameters used in the configuration of the models.

Table 2. Main parameters of the dust models used in this study.

	BSC-DREAM8b	NMMB/BSC-Dust
Meteorological driver	Eta/NCEP	NMMB/NCEP
Model domain	North Africa-Middle East-Europe (25º W – 60º E and 0º – 65º N)	
Initial and boundary conditions	NCEP/GFS data (at 0.5º × 0.5º horizontal resolution) at 12 UT are used as initial conditions and boundary conditions at intervals of 6 hours	
Horizontal resolution	0.33º x 0.33º	
Vertical resolution	24 Eta-layers	40 σ-hybrid layers
Time step	3h	
Dust size bins	8 (0.1–10 μm)	
Radiation interactions	Yes	Yes
Dust initial condition	24 h forecast from the previous day’s model run	

The modeled dust extinction values at 550 nm are directly compared with the observed particle extinction values at 532 nm because of the wavelength proximity and the low spectral extinction dependence of mineral dust (see Section 4). In order to have continuous observations and to maximize their number, day and nighttime inversions of particle backscatter coefficients are used and converted to extinction by multiplying them by a constant lidar ratio of 50 sr. The vertical resolution of both dust models is much coarser than the lidar vertical resolution. In order to evaluate the models' capability to reproduce the vertical distribution of the dust extinction coefficient, the original lidar vertical resolution is downgraded to the resolution of the modeled profiles.

Given that the extinction value at a given height, h_i, of the models is the average extinction of the layer comprised between $h_i - \frac{h_i - h_{i-1}}{2}$ and $h_i + \frac{h_{i+1} - h_i}{2}$, the extinction value of the lidar profile at height h_i is calculated as the mean value of the original lidar profile (at the lidar original vertical resolution) calculated in the exact same layer of each model. For the horizontal resolution, the lidar data can be considered as point observations, while the models represent uniform pixels of 0.33° resolution (~33 km). The temporal resolution is also different: while the models provide instantaneous profiles with a time steps of 3 hours, the lidar profiles are averaged over 30 or 60 min. Here we have compared each modeled profile at time t with a 30- (60-) min. averaged lidar-derived profile included in the interval [$t-30$, $t+29$ min.] ([$t-60$, $t+59$ min.]). In case two consecutive measurements fulfil this criterion, the measurement which was running at time t is selected. The forecast skill analysis is performed in terms of two vertically integrated statistical indicators, namely the fractional bias (FB), and the correlation coefficient (r), as well as in terms of the center of mass (CoM). FB and r are both calculated for the extinction coefficient. The fractional bias is a normalized measure of the mean bias and indicates only systematic errors, which lead to an under/overestimation of the estimated values. The linear correlation coefficient is a measure of the models' capability to reproduce the shape of the aerosol profile. The vertical integration is made from the lowest pair of simultaneously available model and observed values up to 6 km. No lower limit was fixed because of the dust plume proximity to the ground surface. The upper limit was fixed to 6 km because nearly no dust was detected above that height. The CoM was approximated by the particle backscatter weighted altitude as defined in (Mona et al. 2006) who noted that this approximation “exactly coincides with the true center of mass if both composition and size distribution of the particles are constant with the altitude”.

In the following sections we evaluate the model performances for forecasts of 24 hours (Section 5.1) and then we compare these forecasts to longer ones of 48 and 72 h (Section 5.2) to see how the forecast skill behaves as the lead time increases. A forecast (or a lead time) of 24 h represents all forecasts in the range [0; 23h] since the model initialization. 48 and 72 h forecasts represent all forecasts in the range [24; 47h] and [48; 71h] since the model initialization, respectively.

3 Synoptic situation and columnar properties

3.1 Synoptic situation

During the period from 20 to 23 February 2017, the synoptic situation in the IP was dominated by the influence of an anticyclone centered northwest from the Western coast, extending in ridge to South Central Europe and by the existence of a low pressure system, initially centered over Morocco, as illustrated in the ECMWF ERA5 reanalysis of the Geopotential height at 850 hPa at several hours (Fig.1). This low is very likely to be associated to Sharav cyclone (Alpert and Ziv, 1989). The plots presented in Figure 1 also include the surface wind friction velocity (u_*), which is a good indicator of possible dust emissions from deserts (Alfaro and Gomes, 2001; Darmenova et al., 2009 and references therein). It is generally assumed that the dust flux from the surface involves a power law of the wind friction velocity, as well as some parameters that characterize the surface, as the fraction of vegetation, the surface roughness and the soil texture and water content. Significant dust emissions are likely to occur for high friction velocities (above 0.6ms^{-1}), presenting lower sensitivity to land surface parameters (Darmenova et al., 2009).

The Geopotential field at 850 hPa (Fig.1) indicates the persistence of an atmospheric flow advecting air from the central North Africa (Algeria) crossing the IP. On 20 February (Fig 1a) strong u_* values (> 6 ms^{-1}) represented over Algerian Sahara, a major dust source region (Ginoux et al., 2012) are suitable to force dust aerosol emissions (Darmenova et al., 2009). The well-shaped deep low, centered over central Morocco transported air from Algeria to southern Spain. Over the Central and Northern parts of the Peninsula, the dominant wind brings air from central Europe under the anticyclonic circulation. Wind vectors at 850 hPa are not represented in Fig.1 for clearness, though at this level it is reasonable to assume geostrophic wind. The situation maintains very similar in the next day and on the 22 February the low provokes high winds on the western side (central-northern Algeria), which may be seen by the proximity of the isopleths and by the strong values of u_* (Fig. 1c), which indicates strong dust emissions. On 23 February the northward shift of the Moroccan low originated weak precipitation events in several locations in the south of Portugal and Spain, but still transporting air from Algeria to Northeast Spain (~Catalonia). The u_* over the desert regions dropped significantly, hinting at the end of the significant dust emissions. The synoptic conditions changed sharply on 24 February with the passage of a frontal system that affected all the IP (not shown in Fig.1).

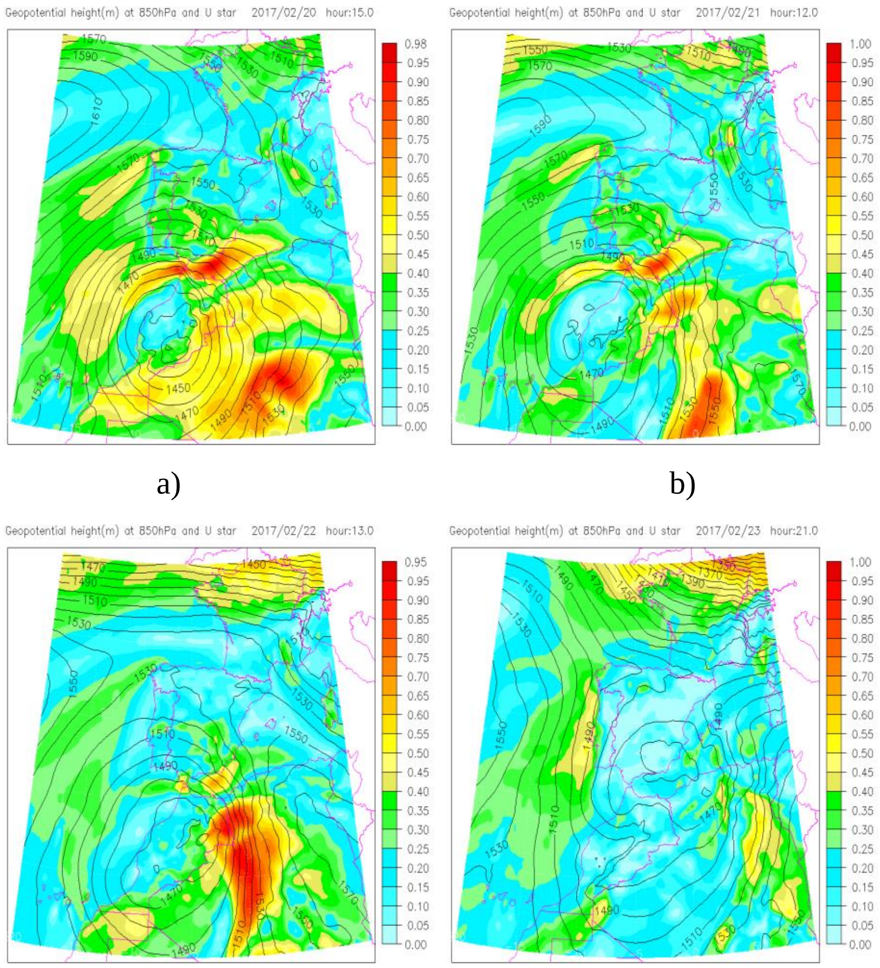

a) b)

c) d)

Fig. 1. European Centre for Medium-Range Weather Forecasts (ECMWF) reanalysis (ERA 5) of the Geopotential height at 850 hPa (black height contours) and surface wind friction velocity (color bar in ms^{-1}) from 20 to 23 February 2017. Generated using Copernicus Atmosphere Monitoring Service information [2018].

Fig. 2 presents RGB composites based upon the combination of infrared channels (8.7, 10.8 and 12.0 μm) from the Spinning Enhanced Visible and InfraRed Imager (SEVIRI) on board Meteosat-10, showing the dust transport evolution (magenta) from 20 to 24 February 2017. The dust was transported across the Alboran Sea (western Mediterranean Sea) and infiltrated in southern Iberian atmosphere on 20 February (Fig.2a), gradually transported towards west and north by the synoptic circulation, affecting the southern and western sites (CR, EV, GR) as illustrated by Figs.2b and 2c. On the 22 February the dust intrusion was reinforced by a thick plume that progressively entered the IP through the southeastern coast (Fig. 2d) extending north and westwards and affecting all sites represented in the images (Fig. 2e). This new intrusion was accompanied by the presence of high clouds that on the 23 February affected most of the IP, associated with the intensification and northward shift of the Moroccan low (Figs.2f and 2g). The arrival of a frontal system from northwest on the 24 February interrupted the North African dust flow, pushing it towards the central Mediterranean regions (Fig. 2h).

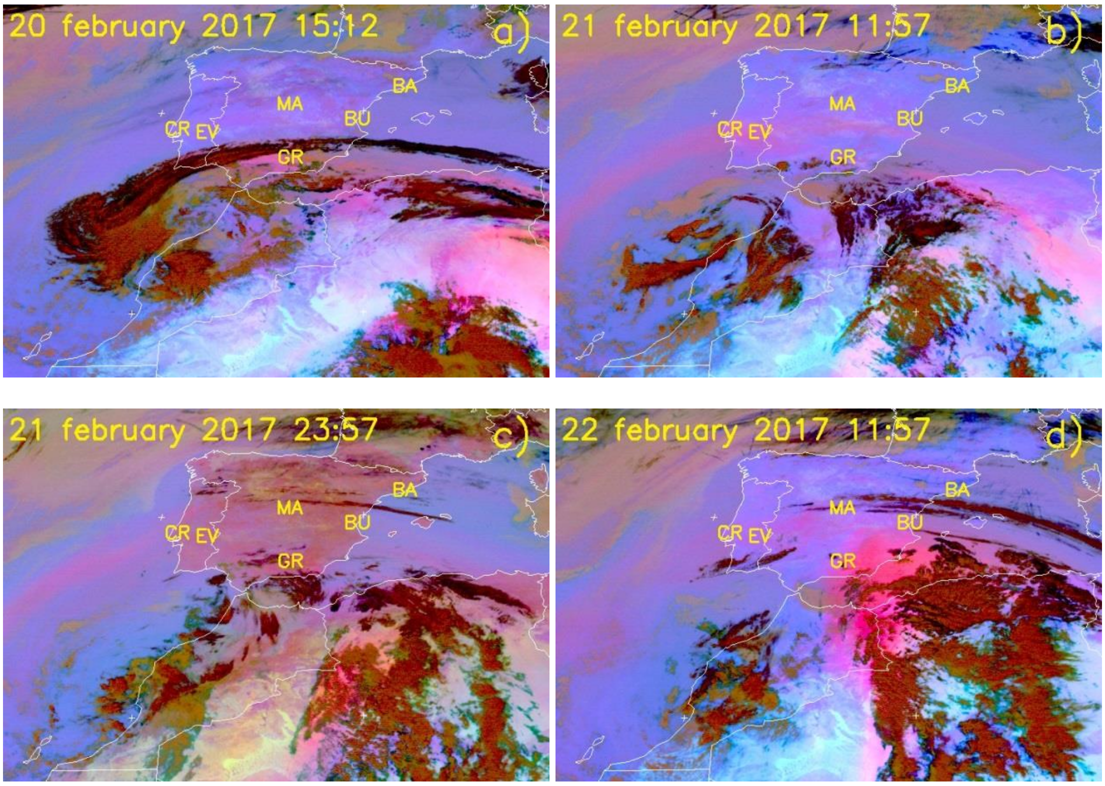

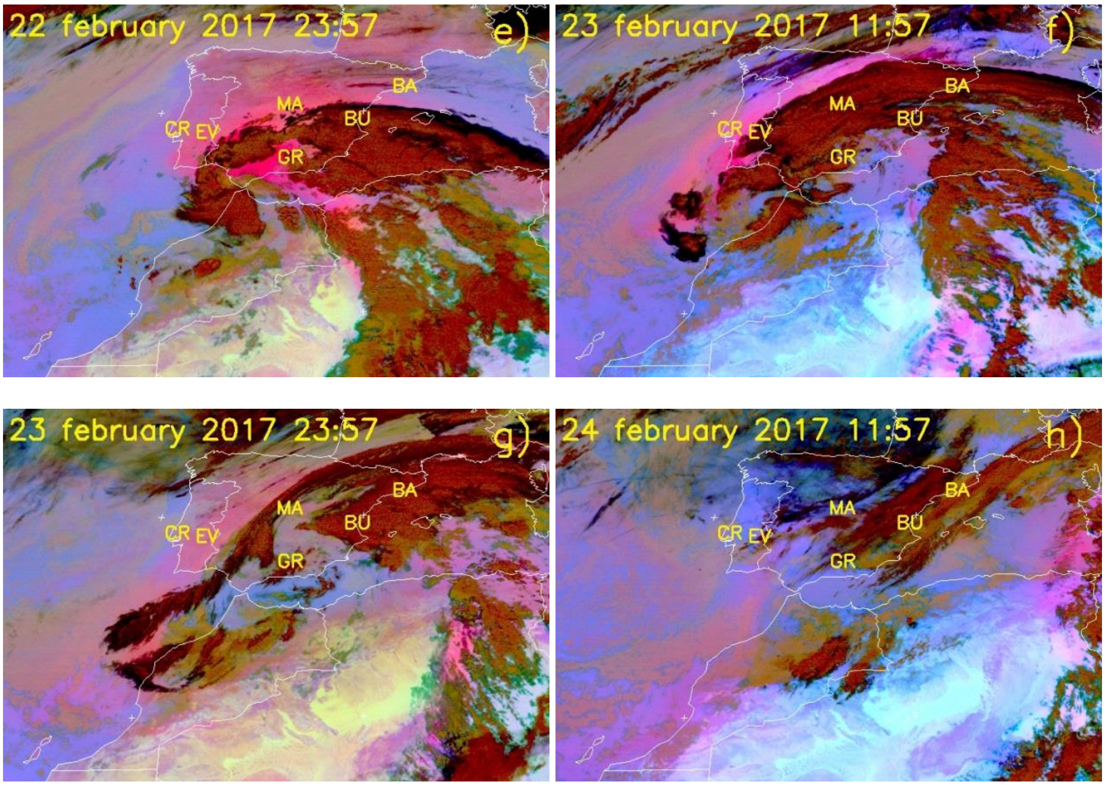

Fig. 2. Meteosat RGB composites showing the evolution of the dust plume from 20 to 24 February 2017. The Iberian sites considered in the study are also represented in the images: Barcelona (BA), Burjassot (BU), Cabo da Roca (CR), Évora (EV), Granada (GR) and Madrid (MA).

The temporal evolution of the back-trajectories, from 20 to 24 February 2017, arriving over the six sites considered, at three atmospheric levels (2000, 3000 and 4000 m a.g.l.) is represented in the supplementary material in Fig. S4. The back-trajectories were calculated using the Hybrid Single-Particle Lagrangian Integrated Trajectory (HYSPLIT) model (Stein et al., 2015; Rolph et al., 2017), available online at http://ready.arl.noaa.gov/HYSPLIT.php. The sequence shows that the first sites overpassed by air masses originating in northern Africa were: Granada (20 February; Fig. S4a), followed by Évora and Cabo da Roca (21 February; Fig. S4b and c). Burjassot and Madrid sites started to be influenced by North African air masses between the 21 and 22 February (Fig. S4d and e) and finally also Barcelona remained under the influence of the same air masses between the 23 and 24 February (Fig. S4f to and h). Information from Meteosat RGB composites (Fig.2) displaying the dust distribution over North African regions and back-trajectories (Fig. S4), hint at dust originating from central Algeria, which is a recognized major dust source region (Ginoux et al., 2012). This is also in agreement with the strong values of wind friction velocities found over the same region and shown in Fig. 1.

3.2 Columnar properties

The desert dust plume entered the IP from the South on the 20 February, and then it gradually reached the northwest and later on the eastern part of the IP. Fig. 3 shows the time series data of AOD at 675 nm and Ångström exponent (440 and 870 nm), from 20 to 25 February 2017 in six sites distributed across the IP. An increase of the AOD was first noticed in Granada site on the 20 February, where the AOD values reach about 1.5, accompanied by very low values of AE, typical of desert dust intrusions, which is confirmed by the Meteosat composite in Fig. 2a. The dust plume maintains its influence over Granada and extends towards the western part of IP, affecting in the next day also Évora and Cabo da Roca sites, with AOD values ranging between about 0.6 and 1.2, once again with very low AE (<0.2). The dust transport continues and on the 22 February, during daytime, desert dust is detected in all stations except for Barcelona where it is measured in the next day. Still on the 22 February, extremely high AOD values are reached in Granada and Burjassot (> 2.0) and moderately high in Madrid, Évora and Cabo da Roca (0.5<AOD<1.0), with AE values lower than 0.2 for all these stations. On the 23 February there are only a few AERONET measurements available due to the persistence of clouds over the region, nevertheless the AOD is still considerably high (>2.0) for Évora and Barcelona, with corresponding AE values around zero in these sites, with the provenience of air masses from desert dust source regions supported by the back-trajectories presented in the supplementary material (Fig. S4). As mentioned before, the frontal system on the 24 February interrupted the dust transport and the AOD values on the 24 and 25 February show a consistent decrease with a corresponding increase of the AE.

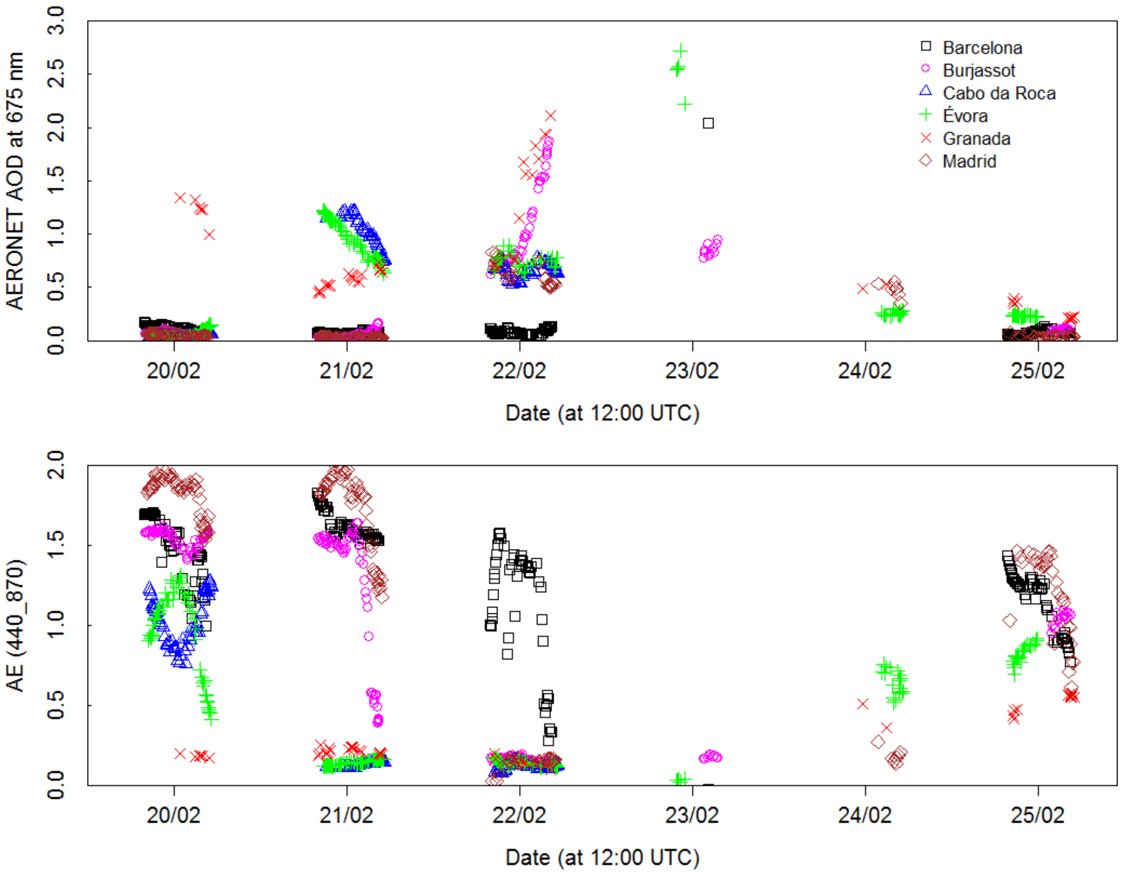

Fig. 3. – AERONET AOD at 675 nm and AE (440 and 870 nm) from 20 to 25 February 2017 in six sites distributed across the IP.

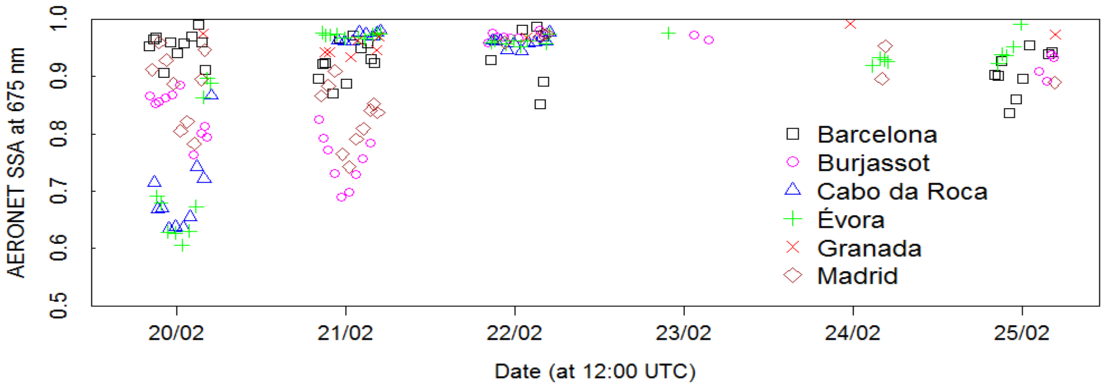

Fig. 4 - AERONET SSA at 675 nm from 20 to 25 February 2017 during the event for six sites distributed across the IP.

The single scattering albedo is characterized by relatively high values in all the stations during the dust event, showing the predominant dispersive nature of these particles. The lower SSA values in the first two days (greater absorption) in some of the sites (BU, CR, EV, MA) depicted in Fig.4, are related with polluted air masses coming from northwestern Europe (not shown here).

4. Vertically-resolved optical properties

ÉVORA

Fig. 5 represents the Range Corrected Signal (RCS) during 4 days, 24 hours per day, which provides a very detailed overview of the phenomenon. It can be seen that the African dust outbreak was especially intense at the beginning of the event, from 20 (12:00 UTC) to 21 (12:00 UTC) February. However, it must be noted that on 21 (12:00 UTC) February a change of the neutral-density filters in front of the detection channel was necessary to be carried out in order to attenuate the received light. This obviously reduced the RCS at this point but did not affect the retrieval of aerosol optical properties. Four different periods have been selected so as to analyze aerosol optical properties from the African plume observed in Évora (highlighted again in red in Fig. 5). Nighttime measurements have been chosen for the analysis in order to estimate accurately such properties given the fact that independent extinction from Raman signals was available at this lidar station. The first period (21st Feb from 0:00-0:30 UTC), presents the highest backscatter coefficient values out of all periods evaluated, so a special attention has been paid to this period (Fig. 6). Notwithstanding the other 3 periods are also analyzed and they can be seen in the supplementary material Fig. S5, S6 and S7. Mean aerosol optical properties are exposed in this latter Table (3) for specific atmospheric layers where in principle the dust plume is representative. For instance, the first period analyzed presents an African dust plume that reaches also 5 km height asl, however maximum values of particle backscatter coefficient are reached at 3222 m asl and from 4 to 5 km asl the presence of African dust is very small according to particle backscatter coefficient profiles. For this reason, it is considered more appropriate to evaluate the atmospheric layer detected between 1.5-3.5 km asl. At this atmospheric layer, backscatter-related Ångström exponent at the wavelength pairs: 532/355, 1064/532 and 1064/355 were found to be 0.08±0.33, 0.62±0.04 and 0.42±0.13 respectively and the extinction-related Ångström exponent at 532/355 nm was estimated to be 0.16±0.45. These small values are typical for dust as previously reported during extreme African dust outbreaks (Mamouri et al. 2016) (Guerrero-Rascado et al. 2009, Preissler et al. 2011). The other periods also show relatively low backscatter-related Ångström exponents and Ångström exponent values, which in principle indicates a large particle size.

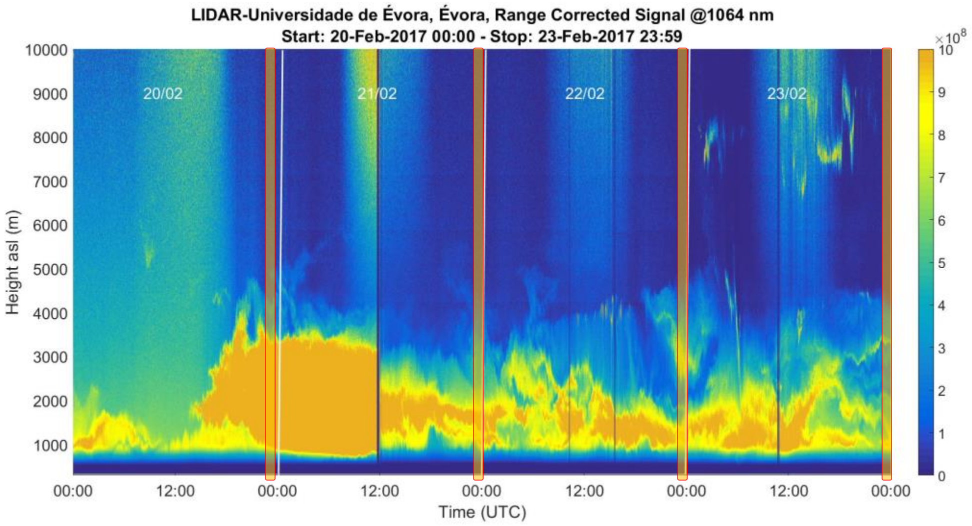

Fig. 5. RCS at 1064 nm on 20-23 February 2017 for the period established between 0:00h-23:59 UTC respectively (Évora, 293 m asl).

Since Raman signals were available and extinction coefficients were obtained independently, particle lidar ratios were derived as well. The dust layer located between 1.5-3.5 km asl on 21Feb (00:00 UTC) presented a lidar ratio of 40±8 sr and 61±18 sr at 355 and 532 nm, respectively. Our estimates at 355 nm are in agreement with Mona et al. that found a mean lidar ratio at 355 nm of 38±15 sr for three years of Raman lidar measurements of Saharan dust (Mona et al. 2006). On the other hand, lidar ratio at 532 nm is found greater than the lidar ratio at 355 nm for the first period analyzed (21 Feb, 00:00 UTC), which is not usual for dust particles as it has been already pointed out by other authors (Muller et al. 2010). Nevertheless, this trend is only observed in the first period analyzed, the other three analyzed periods show a lidar ratio at 532 lower than the lidar ratio at 355 nm. The reason behind this observation (high unexpected lidar ratio values at 532 nm) can be attributed to non-accurate retrievals handicapped by the high aerosol load, which produces great extinction and consequently a scarce lidar signal to be evaluated. It is noteworthy to mention that the standard deviation of the mean lidar ratio at 532 nm on 21Feb (00:00 UTC) is significantly higher compared to the rest of the studied period. On another note, the lidar ratio at 355 nm on 23 Feb (at 00:00 and 23:39 UTC) seems a bit higher than values reported in literature (Mona et al. 2006) and it could be due to a decrease of the African dust outbreak intensity and therefore a greater proportion of local aerosol might be present in the atmosphere. The lidar ratio at 532 nm in all cases (apart from the first period) are consistent with literature since typical values range 35-45 sr for typical desert dust (Mamouri et al. 2013, Nisantzi et al. 2015, Mamouri et al. 2016). In addition, the particle and volume depolarization ratio were 0.19±0.02 and 0.16±0.03 for the aforementioned atmospheric layer on 21Feb 00:00 UTC. These two latter parameters are constant with altitude, which indicates that no changes in the aerosol type is observed within the atmospheric layer of interest. They are also very similar for the four periods studied, however the last period of study indicates lower particle and volume depolarization values that is associated with the decrease of intensity of the Saharan dust outbreak and a greater contribution of local aerosols.

Table 3. Summary of mean aerosol optical properties retrieved for the 4 periods analyzed from Raman lidar measurements (Évora).

Atmospheric layer	LR$_{355}$ (sr)	LR$_{532}$ (sr)	β-AE 1064-532	β-AE 532-355	β-AE 1064-355	AE 532-355	δ-vol.	δ-part.
00:00 UTC-21Feb 1.5-3.5km asl	40±8	61±18	0.62±0.04	0.08±0.33	0.42±0.13	0.16±0.45	0.16±0.03	0.19±0.02
00:00 UTC-22Feb 1.5-4km asl	45±4	38±8	0.76±0.12	-0.12±0.23	0.44±0.08	0.16±0.19	0.16±0.01	0.21±0.01
00:00 UTC-23Feb 1.5-5km asl	52±7	40±9	1.28±0.33	-0.62±0.48	0.58±0.19	0.01±0.27	0.16±0.02	0.19±0.01
23:39 UTC-23Feb 1.5-4.5km asl	55±12	34±8	1.00±0.18	-0.96±0.29	0.28±0.17	0.18±0.24	0.12±0.01	0.15±0.01

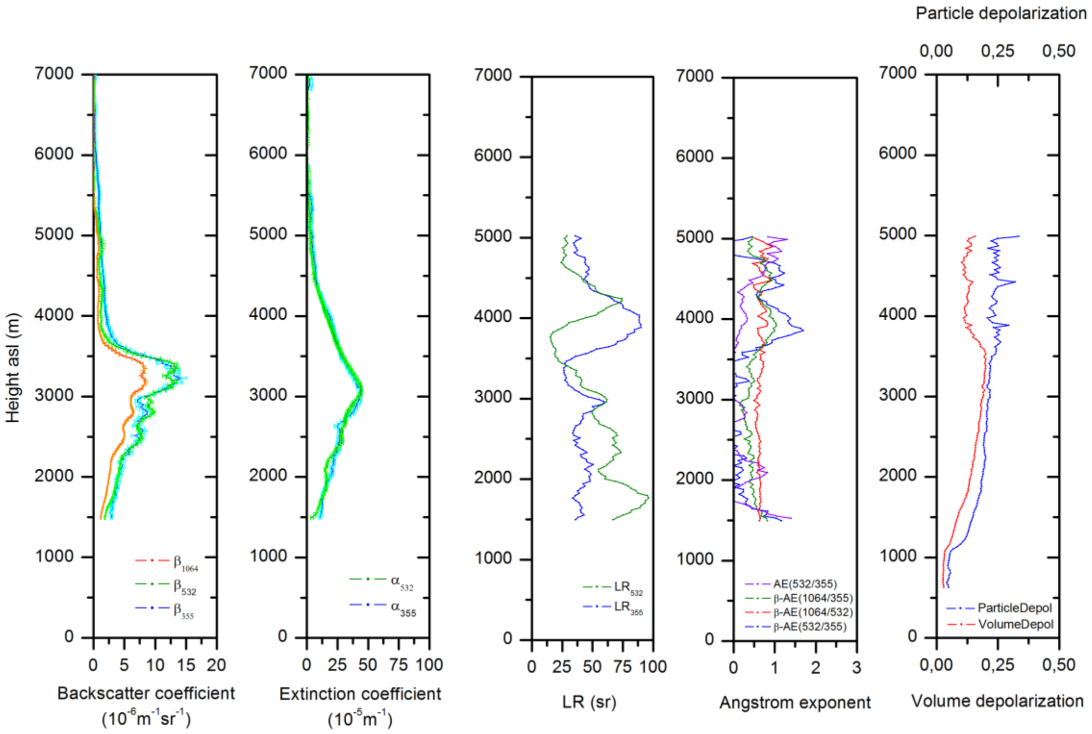

Fig. 6. Backscatter coefficient, extinction coefficient, Lidar ratio, Ångström exponents, and particle and volume depolarization profiles at 00:00 UTC on 21, February 2017 at Évora.

GRANADA

In Granada, four lidar measurements were carried out during the extreme African dust outbreak. In particular for the periods: 12:00-18:00 and 19:00-21:00 UTC on 20 February, 07:31-14:21 UTC on 21 February, and 07:31-20:00 UTC on 22 February. Such measurements are represented in Fig. 7. The red highlights indicate as previously the selected periods where vertically-resolved aerosol optical properties have been derived. Such vertical profiles can be seen in the supplementary material in Fig. S7, S9, S10 and S11. For a better comprehension of these data, mean aerosol optical properties are presented in table 4 for the periods highlighted in red and for the atmospheric layer where the dust plume is registered. In general terms, the maximum altitude of the dust plume was registered at 4 km asl approximately and it was maintained relatively constant throughout the four lidar measurements. For certain periods (13:30-14:21 UTC on 21st Feb) intensification of the RCS is observed at the top of the dust plume, which may indicate cloud formation processes related to mineral dust.

Concerning intensive aerosol optical properties, backscatter-related and extinction-related Ångström exponents were low, in accordance with previous lidar observations, which indicate a large aerosol size. The Raman retrieval could be performed only for the period 19:00-21:00 UTC on 20 February since it was not possible to perform during nighttime on other days. On 22 February, the African dust outbreak was so intense that it produced large extinction and hampered proper retrieval. So, lidar ratios obtained at Granada were 52±7 and 53±6 at 355 and 532 nm respectively. With regard to particle and volume depolarization ratios, these parameters show similar and consistent values to data obtained in the Évora station. Nevertheless, it is noteworthy to mention that the last analyzed period (12:30 UTC on 22nd Feb) exhibits the greatest particle and volume depolarization ratios observed in all lidar stations. These high values point out that a large backscatter signal related to the cross-polarized component is registered, which in turn is produced by non-spherical particles. This is associated to an enlargement on the contribution of mineral dust due to the reinforcement of the dust plume coming from Africa. Such reinforcement of the dust plume was observed on 22 Feb according to the synoptic meteorological situation (see section 3). In fact, it was not possible to retrieve proper lidar products for measurements carried out on 22 Feb from 17:30 UTC on, given the large extinction of radiation produced by the high contribution of mineral dust.

Table 4. Summary of mean aerosol optical properties retrieved for the 4 periods analyzed from Raman lidar measurements (Granada).

Atmospheric layer	LR_{355} (sr)	LR_{532} (sr)	β-AE 1064-532	β-AE 532-355	β-AE 1064-355	AE 532-355	δ-vol.	δ-part.
13:30 UTC-20Feb 2.0-4.0 km asl			0.27±0.12	0.19±0.30	0.24±0.04		0.19±0.03	0.22±0.04
20:00 UTC-20Feb 1.8-4.0 km asl	52±7	53±6	0.19±0.08	0.54±0.21	0.32±0.07	0.51±0.43	0.20±0.02	0.25±0.03
07:31 UTC-21Feb 1.5-3.4km asl			0.86±0.07	0.64±0.13	0.77±0.08		0.18±0.03	0.28±0.01
12:30 UTC-22Feb 1.5-4.0 km asl			0.39±0.12	0.32±0.17	0.36±0.07		0.26±0.01	0.31±0.02

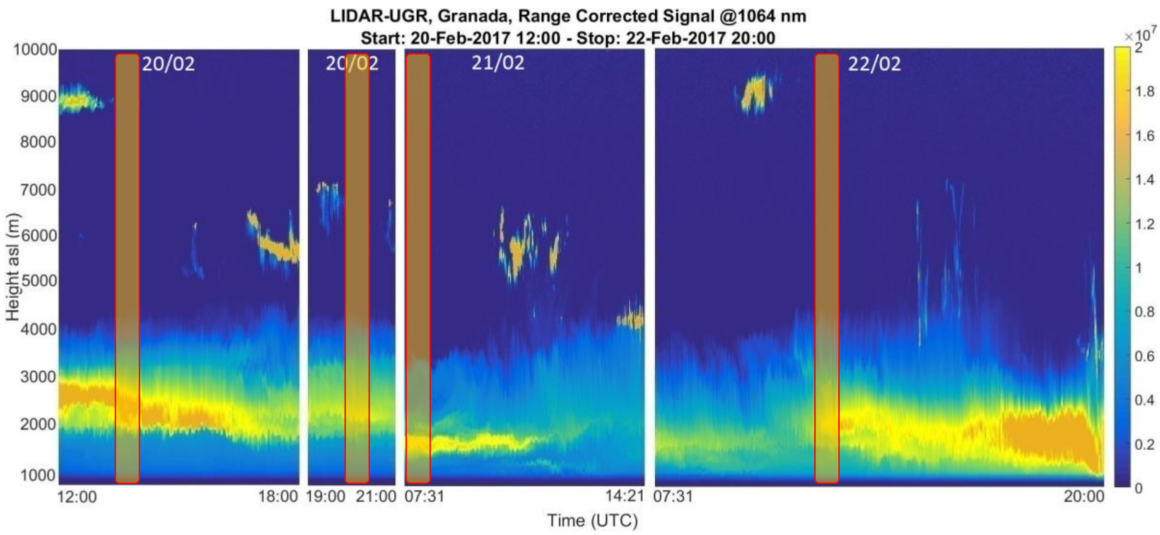

Fig. 7. RCS at 1064 nm on 20 February (12:00-18:00, 19:00-21:00 UTC), 21 February (07:31-14:21 UTC), 22 February (07:31-20:00 UTC) 2017 at Granada (680 m asl).

MADRID

In Madrid, as it occurred in Barcelona, the African dust plume was only detected in the last stage of the African event when the reinforcement of the dust intrusion was produced by synoptic flows (from 22 February on). Lidar measurements on 20 February (not shown) at Madrid still did no present any sign of this extraordinary plume. During this African event, three lidar measurements were available at this station: on 22 Feb (21:00-23:36 UTC) and 23 Feb (05:00-08:00 and 11:00-11:52 UTC). They are represented in Fig. 8. As it can be seen the thickness of the plume ranged from the ground to 5 km asl and in the last lidar measurement the plume was accompanied by thick clouds. Concerning the retrieval of vertically-resolved aerosol optical properties, only the period 05:00-08:00 UTC (23 Feb) was considered for this purpose. Such profiles are represented in Fig. 9, which concerns the period 06:59-07:29 UTC highlighted in Fig 8. Only one profile is presented given the fact that the extinction observed on the first and third lidar measurement was again excessive at low altitudes due to the dust plume, so Rayleigh extinction could not be appropriately computed. This is a problem we want to highlight as it appeared in several lidar stations when addressing this study and performing the retrievals under such extreme conditions (high aerosol load).

Finally, Fig. 9 presents 3 backscatter coefficient profiles at 1064, 532 and 355 nm and their respective backscatter-related Ångström exponents. No particle extinction coefficients could be obtained independently as Raman signal were too noisy due to the aforementioned reasons. Maximum values of particle backscatter coefficient are reached at 2200-2300 m asl. At this altitude β_{355} is $(6.85\pm0.09)\cdot10^{-6}$, β_{532} is $(6.35\pm0.13)\cdot10^{-6}$ and β_{1064} is $(5.75\pm0.01)\cdot10^{-6}$ $m^{-1}sr^{-1}$. Mean backscatter-related Ångström exponents were found to be 0.52±0.34, 0.28±0.17, 0.37±0.22 at the wavelength pairs: 532/355, 1064/532 and 1064/355 nm for the atmospheric layer established from lidar full overlap height to 4900 m. These low backscatter-related Ångström exponents are in accordance with previous lidar observations, which partially indicate a large aerosol size.

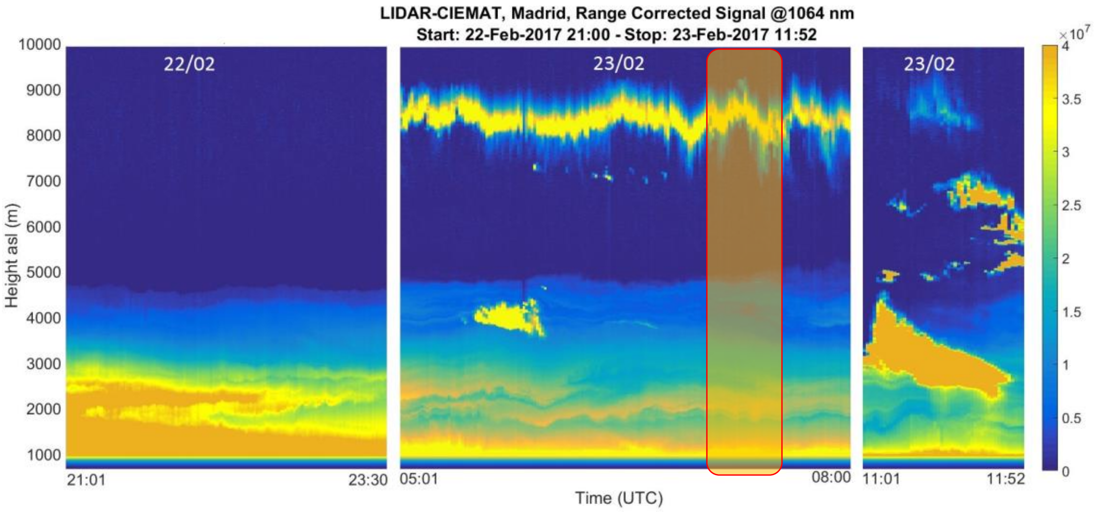

Fig. 8. RCS at 1064 nm on 22 February (21:00-23:36), 23 February (05:01-08:00 UTC), 23 February (11:00-11:52 UTC) 2017 at Madrid (669 m asl)

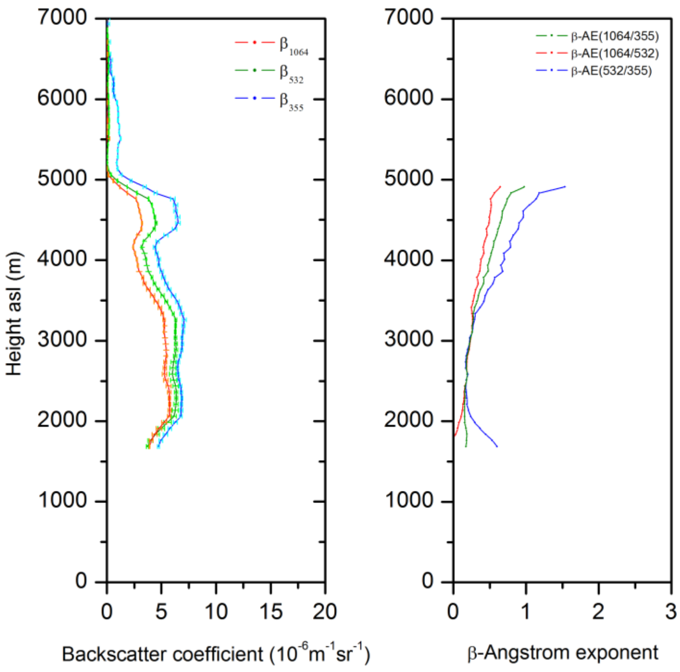

Fig. 9. Backscatter coefficient and β-Ångström exponent profiles at 06:59 UTC on 23 February 2017 at Madrid.

BARCELONA

According to the meteorological overview, the Barcelona site was the latest place from the time standpoint that was hit by the extreme African dust outbreak. As it can be seen in Fig. 10 the African dust plume was registered throughout almost the entire 23 February. At the beginning of the lidar measurement (from 08:11 to 12:00 UTC), the maximum altitude of the plume was detected at 5km asl approximately and after that it decreased gradually until it reached the value of 3-3.5 km at 23:54 UTC. Two periods of 30 minutes have been selected (at 08:11 and 11:34 UTC) to show the retrieval of aerosol optical properties from the lidar measurement. The reason to choose these periods lies on the availability of a clear atmosphere to derive Rayleigh extinction. Both of them are highlighted in red on Fig 10. As indicated in the color bar, the RCS was considerably high for the atmospheric layer between 1 and 3 km during the period 08:11-08:41 UTC. This is one of the reasons why this period of study was selected since in principle this variable is a proxy of the intensity of the African dust outbreak. The second period to be studied spans from 11:34 to 12:04 UTC. In this case, the dust plume is observed up to 5 km asl, although the structure is a bit different and the RCS is lower than in the first period. It must also be noted that from 12:00 UTC on the aerosol optical properties retrieval is quite complex since it is quite difficult to detect a clean atmospheric layer so as to derive the Rayleigh extinction, which is mandatory to infer the aforementioned aerosol optical properties. For the period 12:00-16:00 UTC dispersed clouds can be observed at 5-7 km and from 17:00-18:00 UTC on clouds are registered at the top of the dust plume layer (at 4 km), which prevents the Rayleigh extinction computation. This latter observation is also interesting from the point of view of cloud formation processes. Considering the evolution of the plume throughout the entire lidar measurement at 4 km, it is plausible that African dust aerosol might act as cloud nuclei (see RCS at 4 km from 18:00 to 23:54 UTC, the variable becomes more intense than previously).

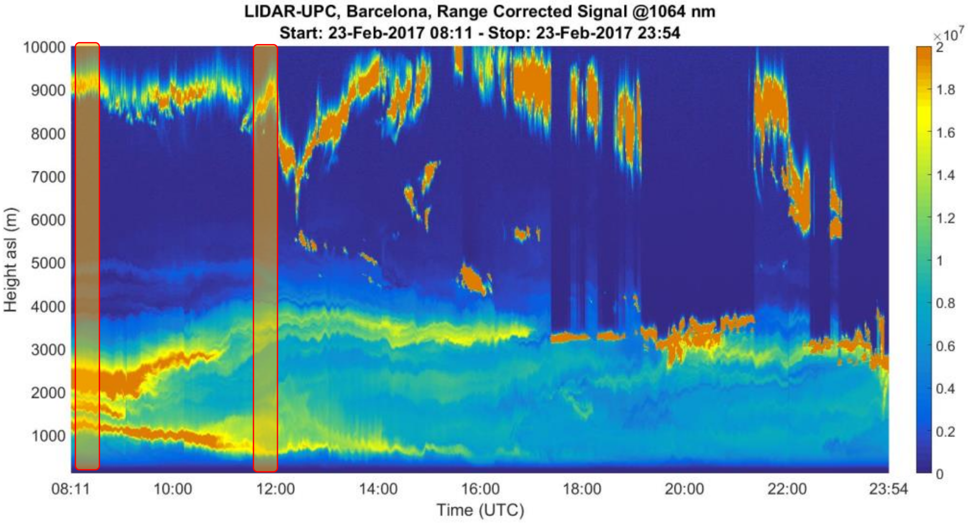

Fig. 10. Range corrected signal (RCS) at 1064 nm on 23 February 2017 for the period established between 08:11-23:54 UTC (Barcelona, 115 m asl).

Fig. 11 shows aerosol optical properties obtained for the period 08:11-8:41 UTC. The left panel represents the vertical profiles of particle backscatter coefficient at the three wavelengths. The maximum values of this variable are reached at 2337 m asl. At this altitude β_{355} is $(1.53 \pm 0.14)\cdot10^{-5}$, β_{532} is $(1.35 \pm 0.04)\cdot10^{-5}$ and β_{1064} is $(0.9 \pm 1.6)\cdot10^{-5}$ $m^{-1}sr^{-1}$. The mean backscatter-related Ångström exponents are 0.37±0.14, 0.45±0.22, 0.42±0.17 respectively at the wavelength pairs: 532/355, 1064/532, 1064/355 for the altitude range 1-3km asl. In general terms, the greater the aerosol size the lower the Ångström exponent. In this case the variable used is the backscatter-related Ångström exponent, which is similar to the previous one (Ångström exponent), so the relation is affected by other parameters such as refractive index, etc. other than the aerosol size.

Nevertheless, these values are typical for African dust (Guerrero-Rascado et al. 2009), where aerosol size plays an important role on this parameter. It is noteworthy to mention that the vertical profile of the backscatter-related Ångström exponent is relatively constant through the atmospheric layer detected between 1-3 km asl. With regard to volume and particle depolarization ratio, we have found mean values of 0.21±0.03 and 0.26±0.01 respectively for the aforementioned atmospheric layer. In addition, a slightly increase of depolarization ratio with altitude is observed. The reason behind it lies on the fact that non-spherical particles tend to produce a higher backscatter signal related to the cross-polarized component and higher depolarization ratios. African dust aerosols are well known as non-spherical particles. So this observation would suggest that at higher altitudes (from 1 to 3 km asl) the mineral dust is purer since depolarization ratios are greater. In relation to Fig. 12 (11:34-12:04 UTC), the aerosol dust plume is a bit weaker than in the previous period. The backscatter coefficient profiles are relatively lower and also the backscatter-related Ångström exponent profiles present higher values which should indicate partially a smaller aerosol size. In this sense, the contribution of the local aerosol may be greater. Considering these observations we can conclude that the intensity of the African dust for this period is lower than the previous one. Volume and particle depolarization ratios for the atmospheric layer situated at 1-3 km asl are similar than in the previous period. The mean values are 0.19±0.01 and 0.28 ±0.02 respectively.

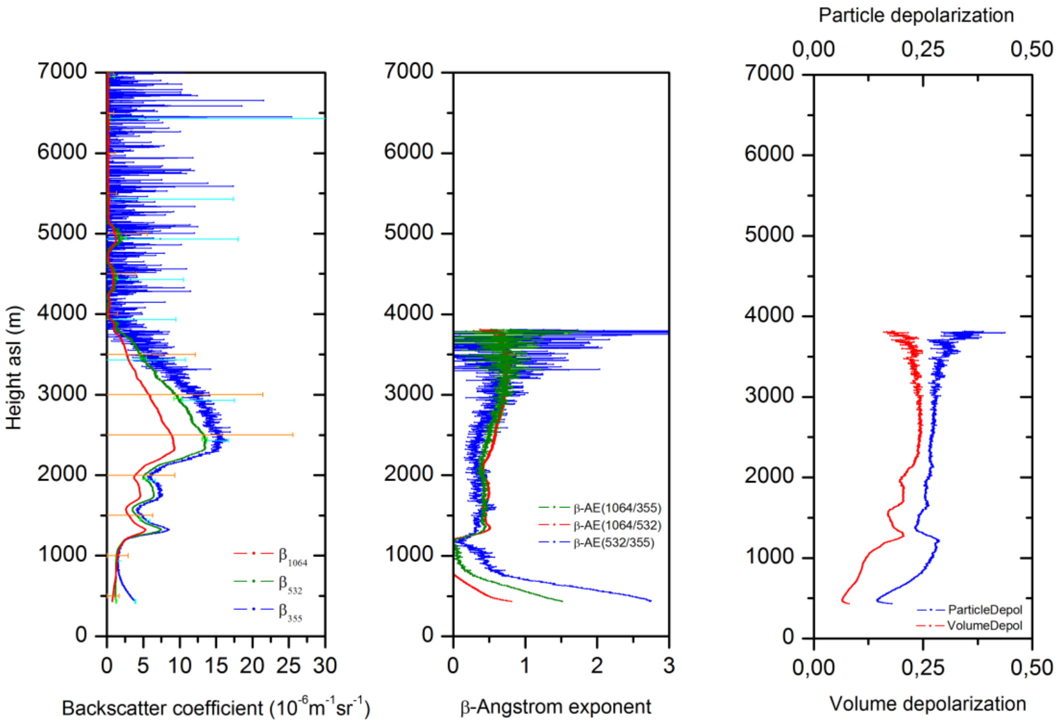

Fig. 11. Backscatter coefficient, β-Ångström exponent, particle and volume depolarization profiles at 08:11 UTC on 23 February 2017.

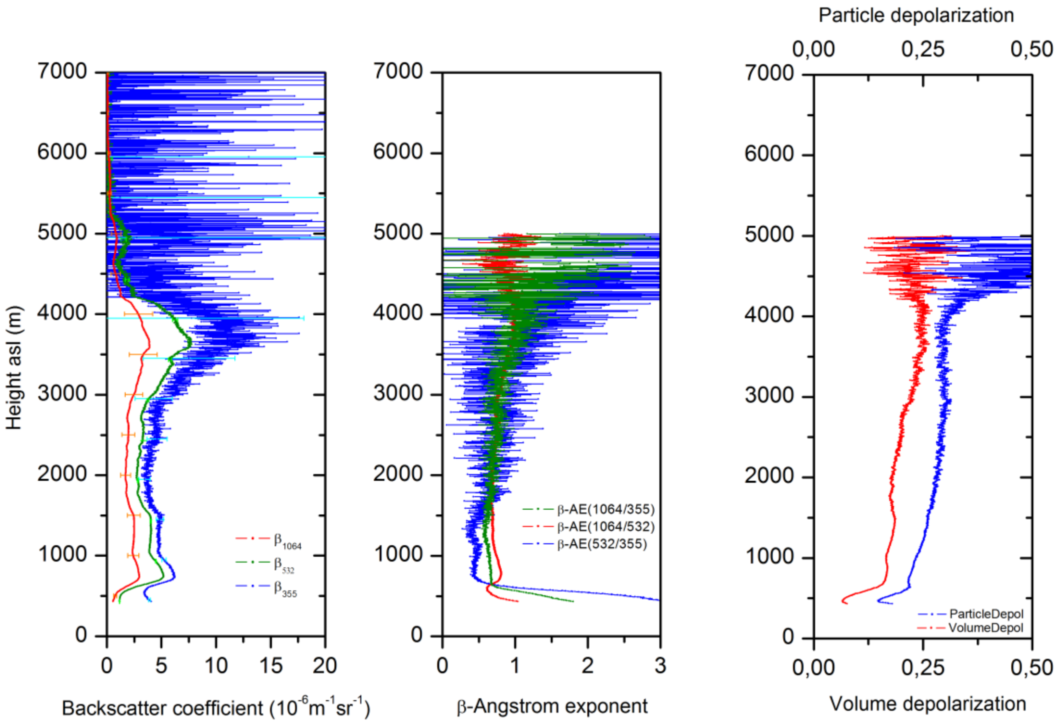

Fig. 12. Backscatter coefficient, β-Ångström exponent, particle and volume depolarization profiles at 11:34 UTC on 23 February 2017.

5 Performance of dust models during intense events

This section aims at examining the performance of dust models to predict the 3D evolution of mineral dust during such intense outbreaks. The literature available on the evaluation of modelled dust vertical profiles usually inspects the behavior of such models on long time series or for a single moderate outbreak (Gobbi et al. 2013, Santos et al. 2013, Mona et al. 2014, Binietoglou et al. 2015, Sicard et al. 2015), and only rarely for intense outbreaks (Huneeus et al. 2016, Ansmann et al. 2017, Tsekeri et al. 2017).

5.1 Forecast skill for a lead time of 24 h

The results are presented for the three sites of Évora, Granada and Barcelona. There are too few measured profiles in Madrid to allow for a statistical comparison. The comparison of the temporal mean profiles of extinction coefficient is made for NMMB/BSC-Dust and BSC-DREAM8b in Fig. 13. The temporal means are averaged over the whole period (see caption of Fig. 13). For each individual profile the correlation coefficient is plotted as a function of fractional bias (FB) in Fig. 14 and the temporal evolution of the latter two parameters is shown in Fig. 15. In the latter figure the time evolution of FB and r is also shown for lead times of 48 and 72 h and discussed in Section 5.2. The mean values of the fractional bias, the correlation coefficient and the center of mass for both models at each site are reported in Table 5.

Table 5 also contains these mean values for lead times of 48 and 72 h, which are discussed in Section 5.2.

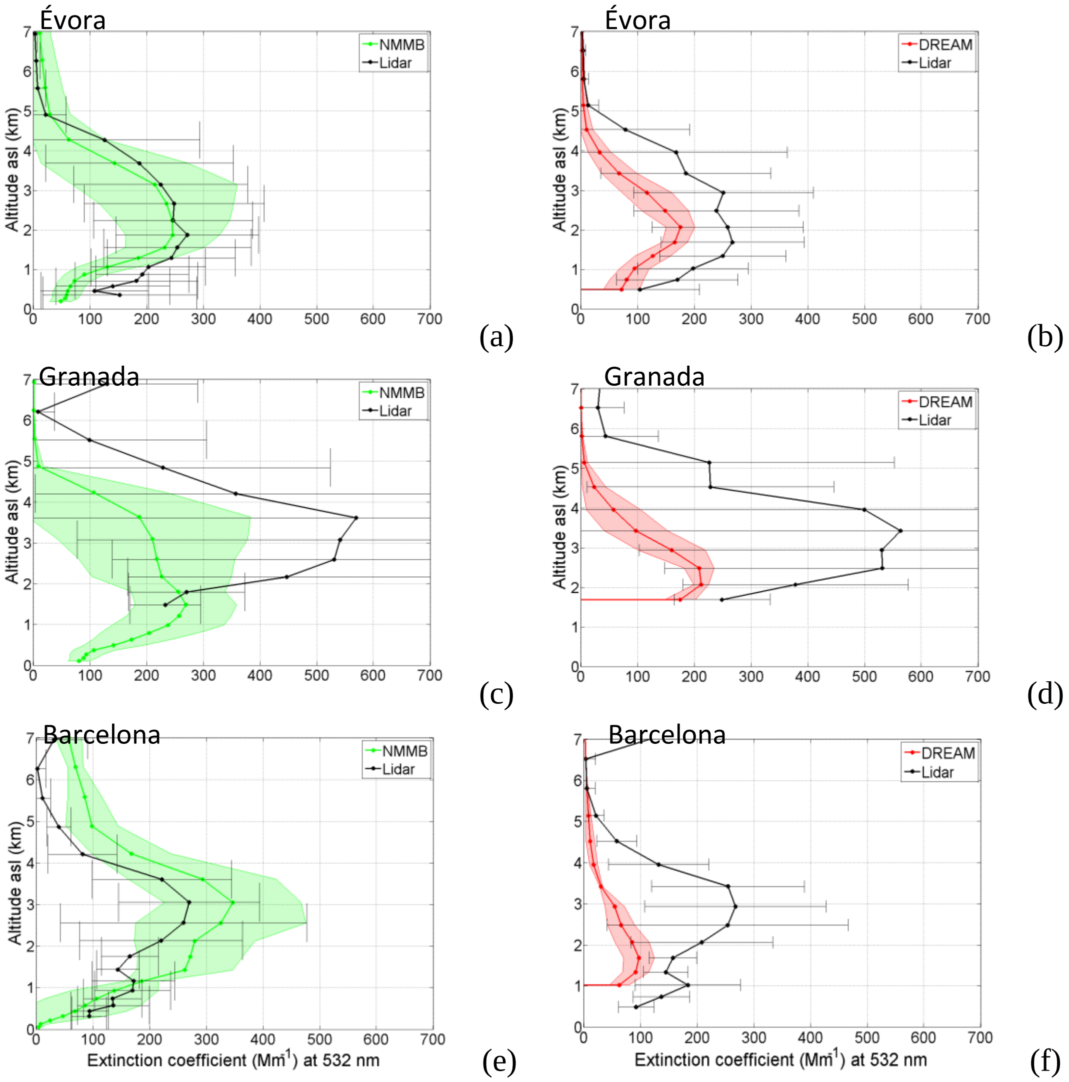

Fig. 13. Mean vertical distribution of mineral dust extinction coefficient estimated by NMMB/BSC-Dust in (a) Évora, (c) Granada and (e) Barcelona and by BSC-DREAM8b in (b) Évora, (d) Granada and (f) Barcelona. The period considered, not always continuous, are 21 Feb. 12UT – 23 Feb. 23UT, 21 Feb. 12UT – 22 Feb. 19UT and 23 Feb. 08UT – 23 Feb. 21UT for Évora, Granada and Barcelona,

respectively. The model shaded areas and the error bars of the lidar represent the standard deviations. All model forecasts are for a lead time of 24 h.

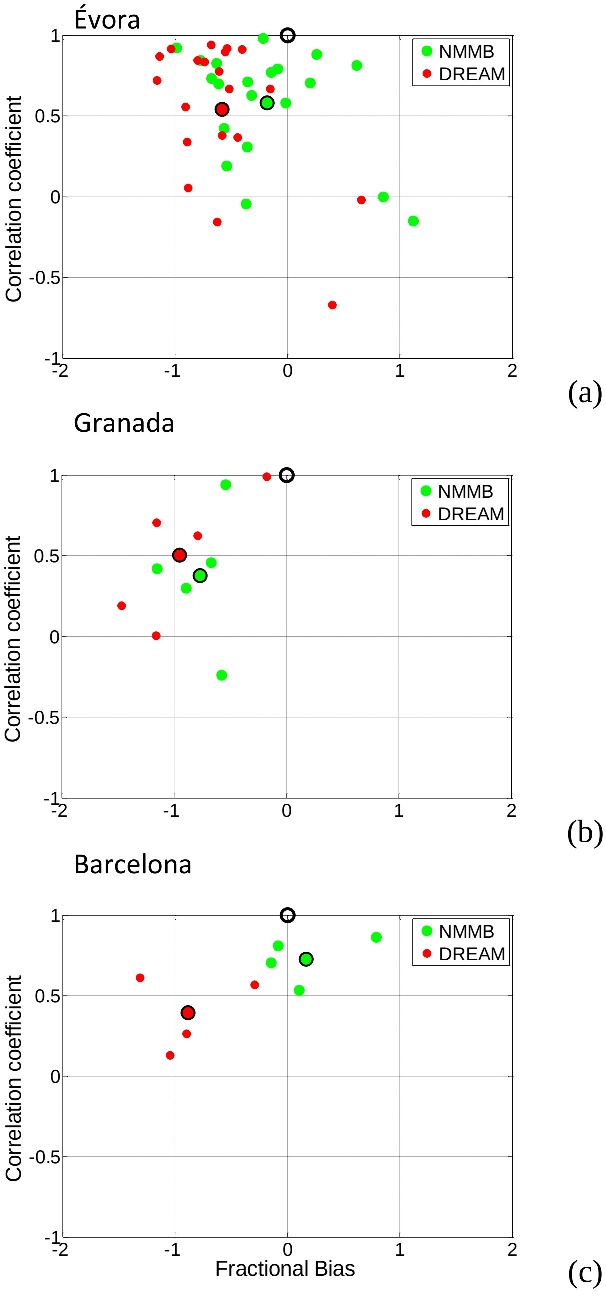

Fig. 14. Correlation coefficient vs. fractional bias, both calculated for the extinction coefficient, calculated for each individual profile in (a) Évora, (b) Granada and (c) Barcelona. All model forecasts are for a lead time of 24 h. The mean values are represented by larger dots edged by a black line. The ideal (FB/r) pair, (0/1), is indicated by a black circle.

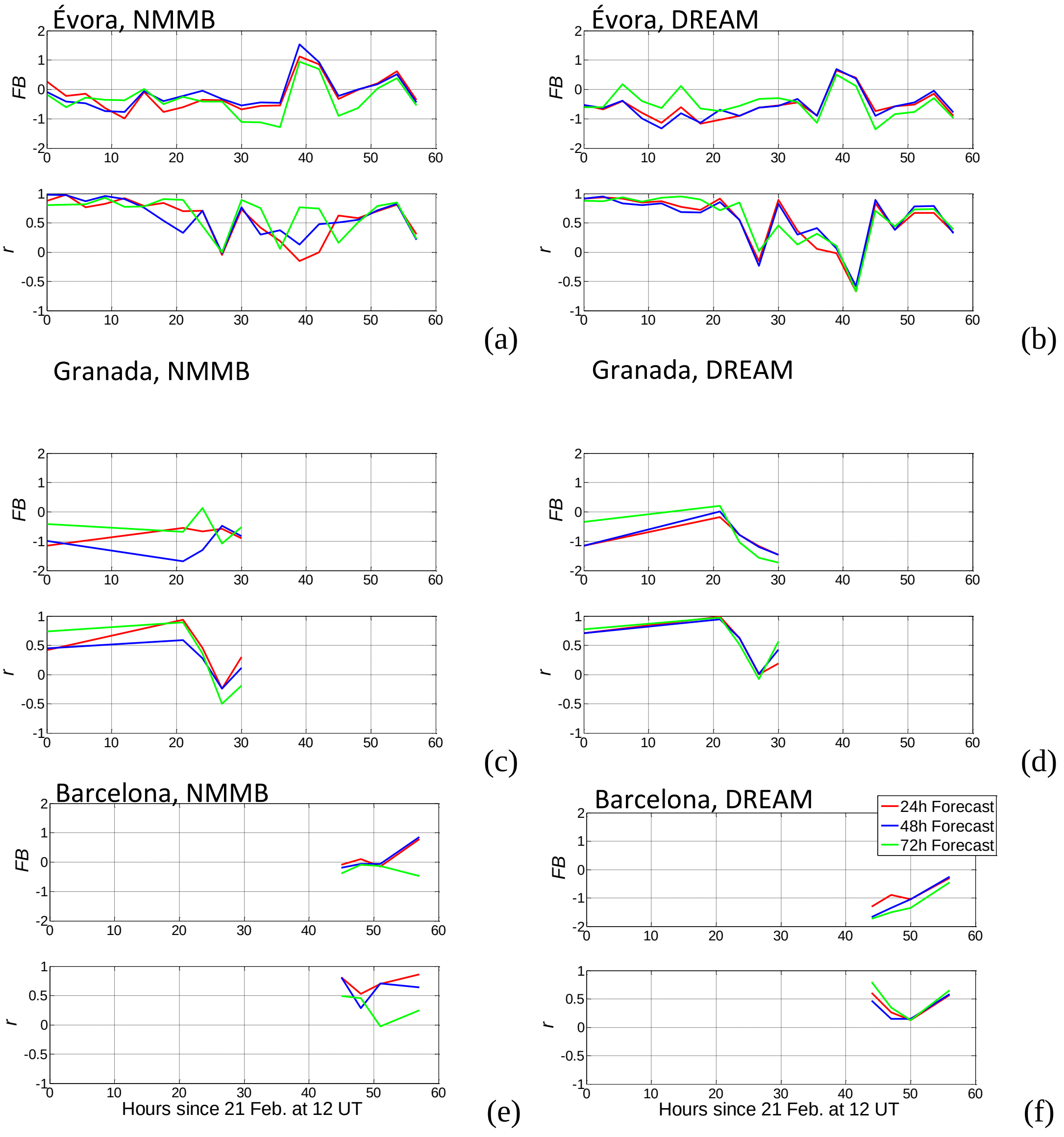

Fig. 15. Correlation coefficient and fractional bias, both calculated for the extinction coefficient, vs. time for forecast lead times of 24, 48 and 72 h for NMMB/BSC-Dust in (a) Évora, (c) Granada and (e) Barcelona and for BSC-DREAM8b in (b) Évora, (d) Granada and (f) Barcelona. The legend shown in the last plot applies to all plots.

Table 5. Main results of the comparison between models and observations. FB and r are both calculated for the extinction coefficient.

	Évora (21 Feb. 12UT – 23 Feb. 23UT)					
	NMMB/BSC-Dust			BSC-DREAM8b		
Number of profiles	20					
Lead time (hours)	24	48	72	24	48	72
FB (%)	-18.0	-12.3	-34.5	-58.0	-57.5	-48.4
r	0.58	0.59	0.65	0.54	0.55	0.56
Model CoM (km)	2.70	2.82	3.04	2.21	2.26	2.38
Lidar CoM (km)	2.43			2.46		

	Granada (21 Feb. 12UT – 22 Feb. 19UT)					
	NMMB/BSC-Dust			BSC-DREAM8b		
Number of profiles	5					
Lead time (hours)	24	48	72	24	48	72
FB (%)	-76.7	-105.5	-50.8	-95.1	-91.6	-89.0
r	0.37	0.24	0.26	0.50	0.54	0.55
Model CoM (km)	2.26	2.38	2.14	2.70	2.79	2.95
Lidar CoM (km)	3.31			3.37		

	Barcelona (23 Feb. 08UT – 23 Feb. 21UT)					
	NMMB/BSC-Dust			BSC-DREAM8b		
Number of profiles	4					
Lead time (hours)	24	48	72	24	48	72
FB (%)	+16.8	+13.8	-26.9	-88.6	-108.0	-126.3
r	0.73	0.61	0.29	0.39	0.34	0.48
Model CoM (km)	3.61	3.72	4.37	2.51	2.53	2.69
Lidar CoM (km)	2.57			2.59		

When looking at the temporal mean profiles of extinction coefficient (Fig. 13), the most striking feature is the general large underestimation of BSC-DREAM8b at all heights independently of the site. This underestimation is smaller in Évora (mean $FB = -48\,\%$, Table 5) than in Barcelona (mean $FB = -88.6\,\%$), where the underestimation is larger. In Fig. 14 it is observed a horizontal spread of the variability of FB larger in Évora ([-115; +65 %]) than in Granada ([-150; -20 %]) and Barcelona ([-130; -30 %]) probably due to the smaller amount of vertical profiles available in Barcelona. The same tendency is observed on NMMB/BSC-Dust data. NMMB/BSC-Dust forecasts show a rather good agreement with the observations, especially in Évora and in Barcelona. While the model tends to underestimate the observations in Évora (especially below the CoM; the mean FB is -18.0 %) and in Granada (especially near the CoM; the mean FB is -76.7 %), it tends to overestimate the observations in Barcelona (especially above 1 km; the mean FB is +16.8 %). The agreement between NMMB/BSC-Dust and the Évora lidar is remarkably good (Fig. 13a), taking into account the atmospheric variability represented by the lidar error bars and the rather long period considered (60 hours). While the NMMB/BSC-Dust profiles reach zero at an approximate height of 5 km in Évora and Granada (similarly to the observations), the profiles in Barcelona start decreasing linearly from ~100 Mm^{-1} at 5 km height to ~50 Mm^{-1} at 7 km (when the observations indicate an extinction coefficient lower than 50 Mm^{-1} above 4.5 km and reaching zero at 6 km). The increase of the lidar profile at 7 km is due to the presence of a cloud above 7 km (see Fig. 10) taken into account in the computation of the layer-average lidar extinction coefficient at the model height. Possible explanations of the differences observed between NMMB/BSC-Dust and the observation in Barcelona in the upper part of the profile are given in the next paragraph. Also in Barcelona the lidar profiles show a layer connected to the surface below 1.5 km, which is not reproduced by either of the models. The main reason is probably the presence of non-dust type particles mixed with the dust detected in the observations but not taken into account in the models. It is also worth noting that BSC-DREAM8b reproduces less atmospheric variability than NMMB/BSC-Dust (in fig. 13, the red shaded areas are smaller than the green ones), whereas the atmospheric variability denoted by the lidar error bars is large at all sites. This seems to indicate that BSC-DREAM8b has less nervousness than NMMB/BSC-Dust.

The capacity of the models to reproduce the shape of the dust vertical distribution is estimated with the correlation coefficient calculated between individual modeled and observed profiles. NMMB/BSC-Dust seems to perform better in Barcelona (r values of 0.73) and in Évora (0.58) than in Granada (0.37). BSC-DREAM8b seems to perform better in Évora (r values of 0.54) and in Granada (0.50) than in Barcelona (0.39). The low r value obtained with BSC-DREAM8b in Barcelona (0.39) is apparently due to a vertical downward transport forecast by the model and not visible from the observations (the peak of BSC-DREAM8b profile is approximately 2 km lower than the peak of the lidar, see Fig. 13f). (Huneeus et al. 2016), who compared NMMB/BSC-Dust and BSC-DREAM8b, among other models, to CALIOP (Cloud Aerosol Lidar with Orthogonal Polarization) profiles during an intense dust outbreak in April 2011 with an AOD ~ 0.8, found a general underestimation of the dust layer height, that was attributed to an overestimation of the dust deposition near the source. The fact that the cloud of points along the r-axis is more spread in Évora (Fig. 14a) than in Granada or Barcelona (Fig. 14b and c) is probably due to the longer time series available in Évora covering two and a half days of the event. Another indicator of the score of the models related to the vertical structure of the dust layer is the center of mass (CoM). In Évora both models retrieve well the center of mass of the dust layers (differences between modeled and observed CoM are less than 0.27 km, see Table 5). In Granada, boths models reproduce smaller CoM values with discrepancies vs. the observations of 1.05 km (NMMB/BSC-Dust) and 0.67 km (BSC-DREAM8b). At this site both models predict a center of mass of the dust plume closer to the ground than it is in reality. In Barcelona BSC-DREAM8b predicts well the CoM with a discrepancy of 0.08 km, The overall performance of BSC-DREAM8b at all three stations are in relatively good agreement with the difference of 0.3±1.0 km found between the same model and the EARLINET station of Potenza, Italy, over a period of 12 years and for dust events with AOD < 0.9 (Mona et al. 2014). In Barcelona, the mean CoM forecasted by NMMB/BSC-Dust is 3.61 km while the lidar measured a mean value of 2.57 km. This large difference is due to the mean NMMB/BSC-Dust profile of extinction in Barcelona which does not reach zero at ~5 km, unlike at the other sites (Fig. 13e; see also the former paragraph). This finding suggests that one or several processes taken into account in NMMB/BSC-Dust and inducing vertical motion of the dust layers did actually not occur. One of these processes is the troposphere–stratosphere exchanges which in some cases has been found to be overestimated by the model because of a misrepresentation of the tropopause that normally limits the maximum altitude of dust transport (Janjic 1994). However, given the limited vertical extension of the dust plume (< 5 km), such an explanation is very unlikely. In our case the vertical upward transport of the dust layers at high altitudes forecast in Barcelona but not in the southern sites is probably due to a too long aerosol lifetime in the upper layers and/or underestimated deposition processes (Mona et al. 2014). Interestingly this overestimation of NMMB/BSC-Dust in the upper layers was also observed by (Binietoglou et al. 2015) who found a slight overestimation of NNMB/BSC-Dust above 4.5-5 km when comparing the model with LIRIC (Lidar/Radiometer Inversion Code) profiles of mass concentration at several sites in

Europe and by (Sicard et al. 2015) who compared the model with profiles from EARLINET stations during a moderate dust event affecting the western Mediterranean Basin in July 2012.

5.2 Forecast skill temporal evolution and comparison for different lead times

The temporal evolution of the score of the models (in terms of FB and r) for different lead times shown in Fig. 15 allows us to evaluate the forecast skill of each model as a function of time since the forecast initialization. The start of the time series is fixed on 21 February, 2017, at 12 UTC, referred in the following as time T_0, when the first observations are available (in Évora and Granada). The observations available allow us to have 20 points of comparison (at a 3-hour time step) from the 21st at 12 UTC until the 23rd at 23 UTC in Évora; 5 points of comparison on the 22nd between 07 and 19 UTC in Granada; and 4 points of comparison on the 23rd between 08 and 21 UTC in Barcelona. In all plots we have represented the temporal evolution of FB and r for lead times of 24, 48 and 72 h. We first discuss the forecast skill temporal evolution for a lead time of 24 h, and then compare it to the evolution at 48 and 72 hours.

In Évora during the first 20 hours (Fig. 15a and b, red lines) both models have similar and more or less stable correlation coefficients with values larger than 0.5. The fractional bias is negative and varies in the range [-100; 0 %]. It is larger (in absolute value) for BSC-DREAM8b than for NNMB/BSC-Dust. At $T_0 + 20$ hours (the 22nd at 08 UTC) the situation starts to degrade: FB variations are larger from one prognostic to the next, especially for NNMB/BSC-Dust, and r passes regularly below the value of 0.5. A few hours before $T_0 + 40$ hours (the 23rd at 04 UTC) and only for a period of 5-6 hours both models overestimate the extinction coefficient ($+50 < FB < +150\,\%$). During the first hours of the 23rd the AOD in Évora reached its highest values (~2.5; see Fig. 3).

In that sense, it seems that the peak of the event is well reproduced in time by the models but its intensity is overestimated. In Granada (Fig. 15c and d, red lines) the prognostic of NNMB/BSC-Dust is quantitatively better (smaller values of FB) but qualitatively worst (smaller correlation coefficients) than for BSC-DREAM8b. Our findings in Granada are in the same line as those found by (Sicard et al. 2015) for a moderate dust event affecting the western Mediterranean Basin in July 2012 who also found that NNMB/BSC-Dust reproduced quantitatively better the profiles while BSC-DREAM8b reproduced better the shape of the profiles. The decrease of FB visible for both models in Granada and starting at $T_0 + 20$ (the 22nd at 08 UTC) coincides with the increase of AOD from ~0.5 to values above 2.0 (see Fig. 3). While on the peak day in Évora (the 23rd) both prognostics show an overestimation for a short period of time, on the peak day in Granada (the 22nd) the general underestimation of both prognostics is accentuated, especially for BSC-DREAM8b. In Barcelona (Fig. 15 e and f, red lines) the comparison starts at $T_0 + 44$ (the 23rd at 08 UTC) at the peak of the event in Barcelona (AOD>2.0, see Fig. 3). NNMB/BSC-Dust shows a very good quantitative agreement in the morning and an overestimation in the afternoon, while BSC-DREAM8b shows an underestimation, which decreases with time. The shape of the vertical profiles is better reproduced by NNMB/BSC-Dust ($r > 0.5$) than by BSC-DREAM8b ($r < 0.5$). In general the forecast skills of BSC-DREAM8b in Barcelona are not as good as those of the southernmost sites. This difference, also observed by (Huneeus et al. 2016) for dust northward transport, might be explained by the difficulties of the models in simulating horizontal winds and vertical dust propagation.

If we now look at the forecast skill as a function of lead time, i.e. at the differences between the red, blue and green lines in Fig. 15, corresponding, respectively, to lead times of 24, 48 and 72 hours, the most striking result is that, at first sight, no clear degradation of the prognostics is clearly visible. There is a difference in the temporal evolution of the prognostics: the prognostics at 24 and 48 h are usually quite similar and the one at 72 h is the one that differs the most from the prognostic at 24 h. But, all in all, if one looks at the overall mean values in Table 6, no clear tendency appears neither in terms of FB, nor r, for Évora and Granada, the two stations closest to the source. In this sense these results are in agreement with those of (Huneeus et al. 2016) who found that the forecast skill of both models for AOD was independent of the forecasting lead time in the domain they defined as southern Europe. In Barcelona a slight degradation of the model scores occurs with increasing lead times: the fractional bias increases (in absolute value; BSC-DREAM8b) and the correlation coefficient decreases (NMMB/BSC-Dust) between the prognostics at 24 and 72 h. This deterioration of the forecast skills is not observed in (Huneeus et al. 2016) and may be due to the singularity and exceptionality of the event described in our study.

6 Conclusions

An extreme dust outbreak transported from Northern Africa to the western Mediterranean during 20-23 February 2017 has been reported and analyzed in the IP. By means of lidar and sun-photometer measurements, we have provided a representative picture of this extreme event by means of a detailed 4-D characterization of aerosol optical properties and their evolution during the African event. Furthermore, the combined use of active and passive remote sensing instruments along with dust models has provided useful information to better understand the complexity of dust long-range transport, its extreme character and also the capability of dust models to forecast such events.

The appearance of the Moroccan low reinforced by the Atlantic anticyclonic system was responsible for the tropospheric flow that advected atmospheric mineral dust over the IP during this extreme event. From the photometry, we would like to remark two main ideas concerning the most intense stages of the event. Firstly, AOD at 675 nm were registered to be around and over 2, the Ångström Exponent (440/870 nm) was close to 0, and SSA was close to 1 in most of AERONET stations, which indicates a high aerosol load, a large aerosol size and the dispersive nature of these particles, characteristics that are attributed to mineral dust. Secondly, the African dust outbreak was accompanied by the presence of clouds that hampered an adequate retrieval and consequently no sun-photometer observations were available at some AERONET stations.

From lidar measurements, the African dust plume could be observed in each lidar station. In general, the altitude range of the plume was observed from the ground until 4-5 km asl approximately at every lidar station. Maximum values of backscatter coefficients at 532 nm were registered by each lidar system in the range $1 - 1.5\cdot10^{-5}m^{-1}sr^{-1}$, where, during the most intense stages the high aerosol load prevented the retrieval, which could not be carried out. This is an issue that also complicated the retrieval in every site. Minimum backscatter-related Ångström exponents at these stages were monitored very close to 0, which are in agreement with the results provided by the sunphotometry. Lidar ratios were found in the range 40 - 55 sr at 355 nm and 34 - 61 sr at 532 nm during the event at Évora and Granada. Particle and volume depolarization ratios, registered at those stations where depolarizing channels were available, have shown an interesting consistency of these values given the fact they were very similar. In general, large particle and volume depolarization ratios are attributed to mineral dust since they are not spherical particles and produce a higher backscatter signal related to the cross-polarized component. The larger the particle and volume depolarization ratios, the purer mineral dust. Likewise, according to these depolarizing properties, lidar systems equipped with this channel have indicated the different structures and aerosol layers throughout the vertical column to distinguish local aerosol from mineral aerosol (for instance in Granada). These findings suggest the need of use of combined instrumentation to characterize adequately aerosol optical properties during this kind of events.

When it comes to forecasting this extreme event, two dust models have been used: BSC-DREAM8b and NMMB/BSC-Dust. According to the fractional bias and the correlation coefficient analysis there is a large underestimation in the forecast of the extinction coefficient provided by BSC-DREAM8b at all heights independently of the site. By contrast, NMMB/BSC-Dust forecasts presented a better agreement with the observations, especially in Évora . However the NMMB/BSC-Dust reproduced a higher atmospheric variability than BSC-DREAM8b. Some discrepancies such as the forecast of dust by NMMB/BSC-Dust in layers well above 5 km are still not completely understood and further research is needed. Finally, with regard to the forecast skill as a function of lead time of each model, no clear degradation of the prognostic is appreciated at 24, 48 and 72h for Évora and Granada stations, however it does for Barcelona, which is in principle attributed to the singularity of the event.

Acknowledgments

The research leading to these results has received funding from ACTRIS-2-H2020 (grant agreement no. 654109) and also from the MINECO (Spanish Ministry of Industry, Economy and Competitiviness) under projects: PROACLIM (CGL2014-52877-R), CRISOL (CGL2017-85344-R, AEI/FEDER), CGL2013-45410-R, CGL2016-81092-R and grant TEC2015-63832-P. Co-funding was also provided by the European

Union through the European Regional Development Fund, included in the COMPETE 2020 (Operational Program Competitiveness and Internationalization) through the ICT project (UID/GEO/04683/2013) with the reference POCI-01-0145-FEDER-007690 and also through ALOP (ALT20-03-0145-FEDER-000004) and DNI-A (ALT20-03-0145-FEDER-000011) projects. This work has also been funded by the research project “Evaluación del impacto en la salud de eventos atmosféricos extremos producidos por el cambio climático" (SINERGIA) and the “Fundación Biodiversidad”, from the Spanish Ministry of Agriculture and Fisheries, Food & Environment (MAPAMA). Measurements in Barcelona were also supported by the European Fund for Regional Development and the Unidad de Excelencia María de Maeztu (grant MDM-2016-0600) funded by the Agencia Estatal de Investigación, Spain. The authors express gratitude to the Juan de la Cierva-Formación program (grant FJCI-2015-23904) for the support provided. This work was supported by the Andalusia Regional Government through project P12-RNM-2409 as well, and by the University of Granada through “Plan Propio. Programa 9 Convocatoria 2013”. The authors thankfully acknowledge the FEDER program for the instrumentation used in this work. We thank AERONET and Juan Ramón Moreta González, Jose M. Baldasano, Ana Maria Silva, José Antonio Martínez for their effort in establishing and maintaining the Madrid, Barcelona, Évora, Burjassot site, respectively. The authors thank S. Basart and O. Jorba from the Dept. of Earth Sciences of the Barcelona Supercomputing Center for providing the dust model data. The authors gratefully acknowledge the NOAA Air Resources Laboratory (ARL) for the provision of the HYSPLIT transport and dispersion model and/or READY website (http://www.ready.noaa.gov) used in this publication.

References.

Alfaro, S. and L. Gomes (2001). "Modeling mineral aerosol production by wind erosion: Emission intensities and aerosol size distributions in source areas". J. Geophys. Res., 106(D16):18075–1808.

Amiridis, V., D. Balis, E. Giannakaki, A. Stohl, S. Kazadzis, M. Koukouli and P. Zanis (2009). "Optical characteristics of biomass burning aerosols over Southeastern Europe determined from UV-Raman lidar measurements." Atmospheric Chemistry and Physics **9**(7): 2431-2440.

Andreae, M. (1995). "Climate effects of changing atmospheric aerosol levels. In: Henderson-Sellers, A. (Ed), World Survey of Climatology, 16, Future Climate of the World. Elsevier, New York, pp. 341-392."

Ångström, A. (1964). "THE PARAMETERS OF ATMOSPHERIC TURBIDITY." Tellus **16**(1): 64-75.

Ansmann, A., I. Mattis, D. Müller, U. Wandinger, M. Radlach, D. Althausen and R. Damoah (2005). "Ice formation in Saharan dust over central Europe observed with temperature/humidity/aerosol Raman lidar." Journal of Geophysical Research: Atmospheres **110**(D18).

Ansmann, A., F. Rittmeister, R. Engelmann, S. Basart, O. Jorba, C. Spyrou, S. Rémy, A. Skupin, H. Baars and P. Seifert (2017). "Profiling of Saharan dust from the Caribbean to western Africa–Part 2: Shipborne lidar measurements versus forecasts." Atmospheric Chemistry and Physics **17**(24): 14987-15006.

Ansmann, A., U. Wandinger, M. Riebesell, C. Weitkamp and W. Michaelis (1992). "Independent measurement of extinction and backscatter profiles in cirrus clouds by using a combined Raman elastic-backscatter lidar." Applied Optics **31**(33): 7113-7131.

Basart, S., C. Perez, S. Nickovic, E. Cuevas and J. Baldasano (2012). "Development and evaluation of the BSC-DREAM8b dust regional model over Northern Africa, the Mediterranean and the Middle East." Tellus Series B-Chemical and Physical Meteorology **64**.

Binietoglou, I., S. Basart, L. Alados-Arboledas, V. Amiridis, A. Argyrouli, H. Baars, J. Baldasano, D. Balis, L. Belegante, J. Bravo-Aranda, P. Burlizzi, V. Carrasco, A. Chaikovsky, A. Comeron, G. D'Amico, M. Filioglou, M. Granados-Munoz, J. Guerrero-Rascado, L. Ilic, P. Kokkalis, A. Maurizi, L. Mona, F. Monti, C. Munoz-Porcar, D. Nicolae, A. Papayannis, G. Pappalardo, G. Pejanovic, S. Pereira, M. Perrone, A. Pietruczuk, M. Posyniak, F. Rocadenbosch, A. Rodriguez-Gomez, M. Sicard, N. Siomos, A. Szkop, E. Terradellas, A. Tsekeri, A. Vukovic, U. Wandinger and J. Wagner (2015). "A methodology for investigating dust model performance using synergistic EARLINET/AERONET dust concentration retrievals." Atmospheric Measurement Techniques **8**(9): 3577-3600.

Boucher, O., Randall, D., Artaxo, P., Bretherton, C., Feingold, G.,, P. Forster, Kerminen, V.-M., Kondo, Y., Liao, H., Lohmann, U.,, P. Rasch, Satheesh, S. K., Sherwood, S., Stevens, B., and Zhang,, i. X. Y.:, edited by: Stocker, T. F., Qin, D., Plattner, G.-K., Tignor,, A. M., S. K., Boschung, J., Nauels, A., Xia, Y., Bex, V., and P. M. and Midgley (2013). Clouds and Aerosols. Climate Change 2013: The Physical Science Basis. Cambridge, United Kingdom and New York, NY, USA**:** 571–657.

Cazorla, A., J. A. Casquero-Vera, R. Román, J. L. Guerrero-Rascado, C. Toledano, V. E. Cachorro, J. A. G. Orza, M. L. Cancillo, A. Serrano, G. Titos, M. Pandolfi, A. Alastuey, N. Hanrieder and L. Alados-Arboledas (2017). "Near real time processing of ceilometer network data: characterizing an extraordinary dust outbreak over the Iberian Peninsula." Atmos. Chem. Phys. Discuss. **2017**: 1-28.

Cuevas, E., A. J. Gómez-Peláez, S. Rodríguez, E. Terradellas, S. Basart, R. D. Garcia, O. E. Garcia and S. Alonso-Perez (2017). "The pulsating nature of large-scale Saharan dust transport as a result of interplays between mid-latitude Rossby waves and the North African Dipole Intensity." Atmospheric Environment **167**: 586-602.

Darmenova K., I. N. Sokolik, Y. Shao, B. Marticorena, G. Bergametti, 2009: "Development of a physically-based dust emission module within the Weather Research and Forecasting (WRF) model: Assessment of dust emission parameterizations and input parameters for source regions in Central and East Asia", J. Geophys. Res., 114, D14201.

Díaz, J., C. Linares, R. Carmona, A. Russo, C. Ortiz, P. Salvador and R. M. Trigo (2017). "Saharan dust intrusions in Spain: health impacts and associated synoptic conditions." Environmental research **156**: 455-467.

Fernald, F. G. (1984). "Analysis of Atmospheric Lidar Observations - Some Comments." Applied Optics **23**(5): 652-653.

Forster, P., V. Ramaswamy, P. Artaxo, T. Berntsen, R. Betts, D. Fahey, J. Haywood, J. Lean, D. Lowe, G. Myhre, J. Nganga, G. Prinn, G. Raga, M. Schulz and R. Van Dorland (2007). "Changes in atmospheric constituents and in radiative forcing." Climate Change 2007: The physical Science Basis, 129-234, Cambridge Univ. Press, U.K.

Ginoux, P., J.M. Prospero, T.E. Gill, N.C. Hsu, M. Zhao (2012). "Global-scale attribution of anthropogenic and natural dust sources and their emission rates based on MODIS Deep Blue aerosol products". Rev. Geophys, 50.

Gobbi, G., F. Angelini, F. Barnaba, F. Costabile, J. Baldasano, S. Basart, R. Sozzi and A. Bolignano (2013). "Changes in particulate matter physical properties during Saharan advections over Rome (Italy): a four-year study, 2001-2004." Atmospheric Chemistry and Physics **13**(15): 7395-7404.

Guerrero-Rascado, J., F. Olmo, I. Aviles-Rodriguez, F. Navas-Guzman, D. Perez-Ramirez, H. Lyamani and L. Arboledas (2009). "Extreme Saharan dust event over the southern Iberian Peninsula in september 2007: active and passive remote sensing from surface and satellite." Atmospheric Chemistry and Physics **9**(21): 8453-8469.

Guerrero-Rascado, J., B. Ruiz and L. Alados-Arboledas (2008). "Multi-spectral Lidar characterization of the vertical structure of Saharan dust aerosol over southern Spain." Atmospheric Environment **42**(11): 2668-2681.

Holben, B., T. Eck, I. Slutsker, D. Tanre, J. Buis, A. Setzer, E. Vermote, J. Reagan, Y. Kaufman, T. Nakajima, F. Lavenu, I. Jankowiak and A. Smirnov (1998). "AERONET - A federated instrument network and data archive for aerosol characterization." Remote Sensing of Environment **66**(1): 1-16.

Holben, B., D. Tanre, A. Smirnov, T. Eck, I. Slutsker, N. Abuhassan, W. Newcomb, J. Schafer, B. Chatenet, F. Lavenu, Y. Kaufman, J. Castle, A. Setzer, B. Markham, D. Clark, R. Frouin, R. Halthore, A. Karneli, N. O'Neill, C. Pietras, R. Pinker, K. Voss and G. Zibordi (2001). "An emerging ground-based aerosol climatology: Aerosol optical depth from AERONET." Journal of Geophysical Research-Atmospheres **106**(D11): 12067-12097.

Huneeus, N., S. Basart, S. Fiedler, J.-J. Morcrette, A. Benedetti, J. Mulcahy, E. Terradellas, C. P. Garcia-Pando, G. Pejanovic and S. Nickovic (2016). "Forecasting the northern African dust outbreak towards Europe in April 2011: a model intercomparison." Atmospheric chemistry and physics **16**(8): 4967.

IPCC (2013). "Summary for Policymakers. In: Climate Change 2013: The Physical Science Basis. Contribution of Working Group I to the Fifth Assessment Report of the Intergovernmental Panel on Climate Change, edited by Stocker, T.F., D. Qin, G.-K. Plattner, M. Tignor, S.K. Allen, J. Boschung, A. Nauels, Y. Xia, V. Bex and P.M. Midgley. Cambridge University Press, Cambridge, United Kingdom and New York, NY, USA.".

Janjic, Z. (1994). "THE STEP-MOUNTAIN ETA COORDINATE MODEL - FURTHER DEVELOPMENTS OF THE CONVECTION, VISCOUS SUBLAYER, AND TURBULENCE CLOSURE SCHEMES." Monthly Weather Review **122**(5): 927-945.

Karanasiou, A. , N. Moreno, T. Moreno, M. Viana, F. de Leeuw, X. Querol (2012). "Health effects from Sahara dust episodes in Europe: Literature review and research gaps."Environment International,Volume 47, Pages 107-114.

Klein, H., S. Nickovic, W. Haunold, U. Bundke, B. Nillius, M. Ebert, S. Weinbruch, L. Schuetz, Z. Levin and L. A. Barrie (2010). "Saharan dust and ice nuclei over Central Europe." Atmospheric Chemistry and Physics **10**(21): 10211-10221.

Klett, J. D. (1981). "Stable Analytical Inversion Solution for Processing Lidar Returns." Applied Optics **20**(2): 211-220.

Lafontaine, C., R. Bryson and W. Wendland (1990). "AIRSTREAM REGIONS OF NORTH-AFRICA AND THE MEDITERRANEAN." Journal of Climate **3**(3): 366-372.

Mahowald, N., A. Baker, G. Bergametti, N. Brooks, R. Duce, T. Jickells, N. Kubilay, J. Prospero and I. Tegen (2005). "Atmospheric global dust cycle and iron inputs to the ocean." Global Biogeochemical Cycles **19**(4).

Mamouri, R., A. Ansmann, A. Nisantzi, P. Kokkalis, A. Schwarz and D. Hadjimitsis (2013). "Low Arabian dust extinction-to-backscatter ratio." Geophysical Research Letters **40**(17): 4762-4766.
Mamouri, R., A. Ansmann, A. Nisantzi, S. Solomos, G. Kallos and D. Hadjimitsis (2016). "Extreme dust storm over the eastern Mediterranean in September 2015: satellite, lidar, and surface observations in the Cyprus region." Atmospheric Chemistry and Physics **16**(21): 13711-13724.

Mona, L., A. Amodeo, M. Pandolfi and G. Pappalardo (2006). "Saharan dust intrusions in the Mediterranean area: Three years of Raman lidar measurements." Journal of Geophysical Research-Atmospheres **111**(D16).

Mona, L., N. Papagiannopoulos, S. Basart, J. Baldasano, I. Binietoglou, C. Cornacchia and G. Pappalardo (2014). "EARLINET dust observations vs. BSC-DREAM8b modeled profiles: 12-year-long systematic comparison at Potenza, Italy." Atmospheric Chemistry and Physics **14**(16): 8781-8793.

Muller, D., A. Ansmann, V. Freudenthaler, K. Kandler, C. Toledano, A. Hiebsch, J. Gasteiger, M. Esselborn, M. Tesche, B. Heese, D. Althausen, B. Weinzierl, A. Petzold and W. von Hoyningen-Huene (2010). "Mineral dust observed with AERONET Sun photometer, Raman lidar, and in situ instruments during SAMUM 2006: Shape-dependent particle properties." Journal of Geophysical Research-Atmospheres **115**.

Muller, D., B. Heinold, M. Tesche, I. Tegen, D. Althausen, L. Arboledas, V. Amiridis, A. Amodeo, A. Ansmann and D. Balis (2009). "EARLINET observations of the 14-22-May long-range dust transport event during SAMUM 2006: validation of results from dust transport modelling." TELLUS. SERIES B, CHEMICAL AND PHYSICAL METEOROLOGY **61**(1): 325-339.

Nisantzi, A., R. Mamouri, A. Ansmann, G. Schuster and D. Hadjimitsis (2015). "Middle East versus Saharan dust extinction-to-backscatter ratios." Atmospheric Chemistry and Physics **15**(12): 7071-7084.

Obregón, M., S. Pereira, V. Salgueiro, M. J. Costa, A. M. Silva, A. Serrano and D. Bortoli (2015). "Aerosol radiative effects during two desert dust events in August 2012 over the Southwestern Iberian Peninsula." Atmospheric Research **153**: 404-415.

Pappalardo, G., A. Amodeo, A. Apituley, A. Comeron, V. Freudenthaler, H. Linne, A. Ansmann, J. Bosenberg, G. D'Amico, I. Mattis, L. Mona, U. Wandinger, V. Amiridis, L. Alados-Arboledas, D. Nicolae and M. Wiegner (2014). "EARLINET: towards an advanced sustainable European aerosol lidar network." Atmospheric Measurement Techniques **7**(8): 2389-2409.

Pappalardo, G., A. Amodeo, M. Pandolfi, U. Wandinger, A. Ansmann, J. Bosenberg, V. Matthias, V. Amirdis, F. De Tomasi, M. Frioud, M. Iarlori, L. Komguem, A. Papayannis, F. Rocadenbosch and X. Wang (2004). "Aerosol lidar intercomparison in the framework of the EARLINET project. 3. Raman lidar algorithm for aerosol extinction, backscatter, and lidar ratio." Applied Optics **43**(28): 5370-5385.

Perez, C., K. Haustein, Z. Janjic, O. Jorba, N. Huneeus, J. Baldasano, T. Black, S. Basart, S. Nickovic, R. Miller, J. Perlwitz, M. Schulz and M. Thomson (2011). "Atmospheric dust modeling from meso to global scales with the online NMMB/BSC-Dust model - Part 1: Model description, annual simulations and evaluation." Atmospheric Chemistry and Physics **11**(24): 13001-13027.

Perez, C., S. Nickovic, G. Pejanovic, J. Baldasano and E. Ozsoy (2006). "Interactive dust-radiation modeling: A step to improve weather forecasts." Journal of Geophysical Research-Atmospheres **111**(D16).

Pey, J., X. Querol, A. Alastuey, F. Forastiere and M. Stafoggia (2013). "African dust outbreaks over the Mediterranean Basin during 2001–2011: PM 10 concentrations, phenomenology and trends, and its relation with synoptic and mesoscale meteorology." Atmospheric Chemistry and Physics **13**(3): 1395-1410.

Preissler, J., F. Wagner, S. Pereira and J. Guerrero-Rascado (2011). "Multi-instrumental observation of an exceptionally strong Saharan dust outbreak over Portugal." Journal of Geophysical Research-Atmospheres **116**.

Prospero, J., P. Ginoux, O. Torres, S. Nicholson and T. Gill (2002). "Environmental characterization of global sources of atmospheric soil dust identified with the Nimbus 7 Total Ozone Mapping Spectrometer (TOMS) absorbing aerosol product." Reviews of Geophysics **40**(1).

Querol, X., J. Pey, M. Pandolfi, A. Alastuey, M. Cusack, N. Pérez, T. Moreno, M. Viana, N. Mihalopoulos and G. Kallos (2009). "African dust contributions to mean ambient PM10 mass-levels across the Mediterranean Basin." Atmospheric Environment **43**(28): 4266-4277.

Salvador, P., S. M. Almeida, J. Cardoso, M. Almeida-Silva, T. Nunes, M. Cerqueira, C. Alves, M. A. Reis, P. C. Chaves, B. Artinano and C. Pio (2016). "Composition and origin of PM_{10} in Cape Verde: Characterization of long-range transport episodes." Atmospheric Environment **127**: 326-339.

Salvador, P., S. Alonso-Perez, J. Pey, B. Artinano, J. de Bustos, A. Alastuey and X. Querol (2014). "African dust outbreaks over the western Mediterranean Basin: 11-year characterization of atmospheric circulation patterns and dust source areas." Atmospheric Chemistry and Physics **14**(13): 6759-6775.

Salvador, P., B. Artíñano, F. Molero, M. Viana, J. Pey, A. Alastuey and X. Querol (2013). "African dust contribution to ambient aerosol levels across central Spain: Characterization of long-range transport episodes of desert dust." Atmospheric Research **127**: 117-129.

Santos, D., M. J. Costa, A. M. Silva and R. Salgado (2013). "Modeling Saharan desert dust radiative effects on clouds." Atmospheric research **127**: 178-194.

Sicard, M., R. Barragan, F. Dulac, L. Alados-Arboledas and M. Mallet (2016). "Aerosol optical, microphysical and radiative properties at regional background insular sites in the western Mediterranean." Atmospheric Chemistry and Physics **16**(18): 12177-12203.

Sicard, M., G. D'Amico, A. Comeron, L. Mona, L. Alados-Arboledas, A. Amodeo, H. Baars, J. Baldasano, L. Belegante, I. Binietoglou, J. Bravo-Aranda, A. Fernandez, P. Freville, D. Garcia-Vizcaino, A. Giunta, M. Granados-Munoz, J. Guerrero-Rascado, D. Hadjimitsis, A. Haefele, M. Hervo, M. Iarlori, P. Kokkalis, D. Lange, R. Mamouri, I. Mattis, F. Molero, N. Montoux, A. Munoz, C. Porcar, F. Navas-Guzman, D. Nicolae, A. Nisantzi, N. Papagiannopoulos, A. Papayannis, S. Pereira, J. Preissler, M. Pujadas, V. Rizi, F. Rocadenbosch, K. Sellegri, V. Simeonov, G. Tsaknakis, F. Wagner and G. Pappalardo (2015). "EARLINET: potential operationality of a research network." Atmospheric Measurement Techniques **8**(11): 4587-4613.

Rolph, G., Stein, A., and Stunder, B., (2017). "Real-time Environmental Applications and Display sYstem: READY". Environmental Modelling & Software, 95, 210-228.

Sorribas, M., J. Adame, E. Andrews and M. Yela (2017). "An anomalous African dust event and its impact on aerosol radiative forcing on the Southwest Atlantic coast of Europe in February 2016." Science of the Total Environment **583**: 269-279.

Stafoggia, M., S. Zauli-Sajani, J. Pey, E. Samoli, E. Alessandrini, X. Basagaña, A. Cernigliaro, M. Chiusolo, M. Demaria and J. Díaz (2016). "Desert dust outbreaks in Southern Europe: contribution to daily PM10 concentrations and short-term associations with mortality and hospital admissions." Environmental health perspectives **124**(4): 413.

Stein, A.F., Draxler, R.R, Rolph, G.D., Stunder, B.J.B., Cohen, M.D., and Ngan, F., (2015). "NOAA's HYSPLIT atmospheric transport and dispersion modeling system", Bull. Amer. Meteor. Soc., 96, 2059-2077.

Tsekeri, A., A. Lopatin, V. Amiridis, E. Marinou, J. Igloffstein, N. Siomos, S. Solomos, P. Kokkalis, R. Engelmann and H. Baars (2017). "GARRLiC and LIRIC: strengths and limitations for the characterization of dust and marine particles along with their mixtures." Atmospheric Measurement Techniques **10**(12): 4995.

Wagner, F., D. Bortoli, S. Pereira, M. J. Costa, A. SILVA, B. Weinzierl, M. Esselborn, A. Petzold, K. Rasp and B. Heinold (2009). "Properties of dust aerosol particles transported to Portugal from the Sahara desert." Tellus B **61**(1): 297-306.

Weinzierl, B., A. Ansmann, J. Prospero, D. Althausen, N. Benker, F. Chouza, M. Dollner, D. Farrell, W. Fomba, V. Freudenthaler, J. Gasteiger, S. Gross, M. Haarig, B. Heinold, K. Kandler, T. Kristensen, O. Mayol-Bracero, T. Muller, O. Reitebuch, D. Sauer, A. Schafler, K. Schepanski, A. Spanu, I. Tegen, C. Toledano and A. Walser (2017). "THE SAHARAN AEROSOL LONG-RANGE TRANSPORT AND AEROSOL-CLOUD-INTERACTION EXPERIMENT Overview and Selected Highlights." Bulletin of the American Meteorological Society **98**(7): 1427-1451.

Weinzierl, B., D. Sauer, A. Minikin, O. Reitebuch, F. Dahlkötter, B. Mayer, C. Emde, I. Tegen, J. Gasteiger, A. Petzold, A. Veira, U. Kueppers and U. Schumann (2012). "On the visibility of airborne volcanic ash and mineral dust from the pilot´s perspective in flight." Physics and Chemistry of the Earth **45-46**: 87-102.

World Meteorological Organization, W. M. O. (2011). "Weather Extreme in a Changing Climate: Hindsight on Foresight " WMO-No. 1075 (ISBN: 978-92-63-11075-6).